Evolution of the Martian Atmosphere: Results of a Monte Carlo Model of Sputtering

David M. Kass[1] and Yuk L. Yung

150-21, Department of Geological and Planetary Sciences, California Institute of Technology, Pasadena, CA 91125

dkass@gps.caltech.edu

yly@gps.caltech.edu

Received _____; accepted _____

To Appear in Icarus

[1]present address: 169-237, Jet Propulsion Laboratory, California Institute of Technology, 4800 Oak Grove Drive, Pasadena, CA 91109

ABSTRACT

Using a Monte-Carlo model, we determine the sputtering yields for the upper atmosphere of Mars at three different epochs (the present, ~2.5 Gyr ago and ~3.5 Gyr ago). The carbon yield increases from ~ 1 at 3.5 Gyr ago to ~ 2 at present. These yields imply that sputtering is a major loss process for CO_2, especially during the early history of the solar system. Over the same period, the yield of oxygen atoms (from all species) increases from ~ 5.5 to ~ 6.5. Based on the uncertainty in the necessary parameters and sensitivity studies with the model, we estimate that these values are good to within 50%.

When combined with estimates of impacting fluxes of O^+ ions (Luhmann *et al.* 1992), our estimates suggest that Mars has lost ~ 0.8 bars of CO_2 and ~ 50 m H_2O over the last 3.5 Gyr. This is a significant fraction of the CO_2 needed to warm Mars sufficiently to allow for liquid water near the surface (Forget and Pierrehumbert 1997; Haberle 1998). Furthermore, both the CO_2 and the water are large volumes compared to the known Martian reservoirs, indicating the important role sputtering has played in the evolution of the atmosphere of Mars.

Subject headings: MARS, ATMOSPHERE; MARS, CLIMATE; ABUNDANCES, ATMOSPHERES; AERONOMY

1. Introduction

There are several lines of evidence that indicate that the Martian atmosphere has undergone significant change over the history of the planet. One of them is the Martian geomorphology, notably the channels, which appear to indicate that the planet once

had liquid water at or near the surface. This implication is also supported by the large enrichment in deuterium (relative to the Earth and meteorites) in the atmosphere. The enrichment, caused by a fractionating loss of water, implies a more humid past atmosphere. In order to get a humid atmosphere, and water near the surface, it is necessary to warm the surface from its current mean temperature of $\sim$ 220K. The easiest way of doing this is with a thicker atmosphere and an atmospheric greenhouse effect. The fractionation of several stable isotopes, in addition to deuterium, also supports the idea of a thick atmosphere during the early history of Mars.

Although there are questions about how much a greenhouse effect could raise the temperature (Kasting 1991; Haberle 1998), most current models require an atmosphere of at least 0.5 bar of CO_2 in order for liquid water to be near the surface (for example, McKay and Davis (1991); Kieffer *et al.* (1992); Forget and Pierrehumbert (1997); Haberle (1998)). Because the current Martian atmosphere has only 7 mbar of CO_2 and only a small amount of H_2O, an important question is the fate of the early water and CO_2.

There are two major possibilities: either the early atmosphere is sequestered somewhere in the planet (Fanale *et al.* 1982) or it has been lost to space. McElroy (1972) pointed out that the water loss might have been determined by dissociative recombination of $O_2^+ + e$, because H loss by Jeans escape is easily accomplished. However, neither Jeans escape nor dissociative recombination is capable of removing significant amounts of CO_2 over the lifetime of the planet's "contemporary" atmosphere (Shizgal and Arkos 1996). One alternative mechanism for the loss of atmosphere to space is atmospheric sputtering (erosion by impact of energetic atoms and ions). Initial investigations concentrated on sputtering by solar wind particles (Tombrello 1982; Watson 1980). While capable of removing H, the solar wind particles are estimated to remove only the equivalent of the current atmosphere of CO_2 over the age of Mars. The mass difference between the solar wind particles and

the bulk atmosphere makes momentum and energy transfers very inefficient. Energetic exospheric O^+ ions were considered a possible source of heavier particles (Tombrello 1982; Watson 1980), but the actual fluxes were not determined until Luhmann and colleagues (Luhmann and Kozyra 1991; Luhmann *et al.* 1992) modeled them. This process is called indirect solar wind induced sputtering, and it is significantly more effective than direct sputtering at removing CO_2 and other heavy species.

2. Theory

Indirect solar wind induced sputtering occurs on planets that do not have an intrinsic magnetic field (or at least a very weak one). In this case, the solar wind is not stopped by the magnetic field and interacts directly with the upper atmosphere. Sputtering can be broken into two steps (see Figure 1). In the first step, the solar wind interacts with the planetary ionosphere. The Martian ionosphere is predominantly populated by O^+ created through dissociation by extreme ultra-violet (EUV) solar radiation (with a small contribution from other sources). The interplanetary magnetic field, carried along by the solar wind, is draped over Mars and penetrates into the ionosphere since Mars does not have a strong intrinsic field. Through plasma interactions, the solar wind and solar EUV transfer energy to the ionosphere. The draping of the interplanetary magnetic field results in a complex field geometry that, due to temporal and spatial variability, further accelerates the ions. These particles then follow helical trajectories defined by the interplanetary magnetic field. Some of the trajectories miss the atmosphere and the ion is swept away by the solar wind as a pickup ion. But some of the particles impact the upper atmosphere as they are accelerated. When they impact, these particles will have much more energy (around 1 keV) than the escape energy (1.5 eV for a carbon atom).

In the second step, where these accelerated ions impact the upper atmosphere, they

collisionally transfer energy and momentum to the neutral component. They can transfer sufficient energy (and an upward velocity) to other atoms and molecules, allowing them to escape. The sputtering yield is the mean number of particles ejected by each incident O^+. Thus, in order to calculate the flux of particles lost by this type of sputtering, it is necessary to calculate the flux of impacting particles and the sputtering yield.

In their work, Luhmann *et al.* (1992) used an analytical model to determine the sputtering yield for the second part of the process. Their work indicated that the sputtering could remove a small amount of atmosphere (about .14 bars of CO_2), but was not capable of removing a thick atmosphere that could create a warm planet. In this work, we use a Monte-Carlo model to recalculate the expected yield. Combining our new yield with the impacting fluxes calculated by Luhmann *et al.* (1992) allows the total amount of atmosphere lost to be estimated.

3. Model

The Monte-Carlo model operates by impacting individual ions on the atmosphere and then determining their collisional history. By calculating the results for a large number of ions, the model can estimate the mean number of atoms that are lost: the sputtering yield.

The sputtering yield is modeled at three different epochs, the present (or 1 EUV), 2.5 Gyr ago (3 EUV), and 3.5 Gyr ago (6 EUV). Each epoch is defined by the strength of the extreme ultraviolet (EUV) flux as a multiple of the current value. These epochs correspond to the times for which Luhmann *et al.* (1992) have calculated the impacting ion fluxes. We use a different model atmosphere for each epoch. For the purposes of sputtering, there are three important parts to the upper atmosphere. The first is the homosphere (where the atmosphere is well mixed). At the top of the homosphere is the homopause above which

is the diffusive region (where each species assumes its own, mass dependent, scale height). The top of the atmosphere, starting at the exobase, is the exosphere (where the particles can escape without any further collisions). Both the homopause and exobase are zones rather than sharp surfaces and actually extend over several kilometers of altitude; this is especially true when including the various species.

The atmosphere for the present is from Nair *et al.* (1994) (see Figures 2 and 3) and was expanded by isostatically calculating an exosphere for each species. Argon was added to the atmosphere of Nair *et al.* (1994) by assuming a constant mixing ratio up to the homopause and then letting it decrease with its mass dependent scale height. While the isostatic assumption is fairly good for most of the species, it probably fails for H_2 above ~300 km due to dissociation and loss to space, but H_2 in this region does not significantly impact the results of interest. The atmospheres at 3 EUV and 6 EUV are from Zhang *et al.* (1993) and have also been extended vertically (see Figure 4). Due to the nature of sputtering, the process is, at least for major species, independent of the total atmospheric pressure. It will occur at a specific pressure level (near the exobase) depending only on the structure of the upper atmosphere (which is primarily controlled by the local temperature and photochemistry).

In addition to the composition of the target atmosphere, the Monte-Carlo model requires the energy dependent collisional cross section for each possible collision as well as the scattering angles for the resulting particles. Both of these values have been compiled or estimated from several sources (see the appendix for more details). The initial parameters used for the impacting O^+ ions, an impact angle of $\sim 124^\circ$ and an energy of 1 keV, are the mean values derived by Luhmann and Kozyra (1991). One run of the model consists of tracking 10^5 ions. This allows for yields to be calculated with standard errors of a few percent.

For each ion processed, the model tracks each accelerated particle though a cascade of collisions. For each particle that is accelerated in a collision, the model first calculates the location of its next collision based on its current location and direction. The distance traveled is determined randomly, based on the number density and cross sections it encounters on its trajectory. Once the location of the collision is determined, the species involved is randomly selected, weighted by the number densities and cross sections at that location. Knowing the target species, the model determines the result of the collision (the energy and direction of each resulting particle). It uses the scattering phase function for the species involved to constrain the Monte-Carlo calculation of the collision.

Each particle is tracked until its final fate is determined. A particle is considered to be finished under two conditions. The first one is when the kinetic energy of the particle falls below a 1.5 eV threshold. At this point, it no longer has sufficient energy to eject itself or another particle of interest and the remaining energy is assumed to collisionally distribute through the atmosphere, effectively being converted to thermal energy. The second condition is if it leaves the top of the model domain (at this point, it is effectively on a collisionless trajectory). If the particle's energy is above the escape energy for that species, it is assumed to escape. If it is below the escape energy, it is assumed to be on a ballistic trajectory and will be thermalized when it reimpacts the atmosphere.

4. Model Results

The numerical model produces three results of interest. The first is the sputtering yields which can be used to obtain the loss rate and integrated loss. The second result is the partitioning of the impacting O^+'s energy. Finally, the model produces the mean source altitude for each particle.

The yields for each species for each atmosphere are listed in Table 1. The H and H_2 results (from the 1 EUV atmosphere) are not included, primarily because their escape energies are well below the 1.5 eV cutoff threshold and the model values are at best a useless lower limit. Furthermore, other escape processes (notably Jeans escape) are much more efficient at removing hydrogen. All of the results in the upper part of the table are the results for the particular species, thus the row for C is for atomic carbon escaping, as opposed to carbon in CO or CO_2. In the lower part of the table are several rows that calculate the total C, O and N yield. These are useful for computing mass balance on the atmospheric loss processes. The final row of the table contains the total yield (number of escaping atoms, regardless of their species) for each atmosphere (the 1 EUV total yield does not contain the contribution from H or H_2). For the 1 EUV column, the value listed is the mean of 100 model runs (each with 10^5 initial ions). In addition, the numerical model uncertainty (as determined from the 100 runs) is indicated. Each escaping carbon is assumed to represent an escaping CO_2 molecule whose O atoms escape otherwise. Any extra O is considered to come from H_2O dissociated in the lower atmosphere (Nair *et al.* 1994).

The differences between the results for the 6 EUV and 3 EUV atmosphere are slight, but statistically significant. They are primarily due to the difference in mixing ratio between O and CO_2 (see Figure 4) in the two atmospheres at the altitudes where sputtering is occurring. There is also a slight effect due to the differences in the way the mixing ratios change with altitude.

The column in Table 1 labeled pure O is a test atmosphere with only atomic oxygen. It was calculated for comparison against modeling work by Johnson and co-workers (Johnson and Luhmann (1998), personal communication, 1998). The O yield of 2.4 is well below their theoretical upper limit of 6 and agrees reasonably with their numerical model yield of ~ 3.

One of the limiting steps in the the sputtering process is the need to create an upward moving particle from one moving downward. This is controlled by the scattering phase functions (parameterized using the Henyey–Greenstein g factor, see equation A2). Since most simple elastic collisions, such as those for single atoms, are forward scattering (in the atmosphere frame of reference), the loss rates are primarily defined by the few cases where one of the particles scatters through a large angle. Due to the multi-body physics, collisions that dissociate one of the involved molecules are more efficient at this than simple elastic collisions. This implies that the total yield for a pure O atmosphere is unrelated to the yield for a more complex atmosphere.

It is interesting to note that while the carbon comes out both as elemental C as well as CO, very little comes out as CO_2. This is because most collisions that can transfer sufficient energy to allow a molecule to escape also dissociate the CO_2. Most of the CO_2 molecules that dissociate completely to allow atomic C to escape are dissociated over several collisions. An impact with a CO_2 creates a hot CO that dissociates in a subsequent collision.

The energy of the impacting ion is distributed into four categories as the model runs (Table 2). Some of the energy is lost to electronic excitation due to near misses that only electronically excite the target without transferring momentum or kinetic energy. This is the single largest energy sink in the process. Some of the energy is also used to dissociate molecules during collisions. While this absorbs energy, it actually improves the sputtering yield because it is much easier for the fragments to escape than for the whole molecule. The third energy sink is in thermal motion of the atmosphere, particles that still have modest amounts of kinetic energy, but do not have enough to escape (or to cause anything other than hydrogen to escape). For convenience, the energy in ballistic particles, only a few eV, is also included in this category. They will thermalize when they re-enter the atmosphere. The remainder of the energy (15% to 20%) is the kinetic energy of escaping particles. These

are the actual sputtered atoms and molecules that are lost to space.

Figures 5–7 show the distributions of altitudes that the various species come from. Each figure is for one of the epochs and plots the distribution of escape altitudes for each species, normalized to the total yield of that species. The dashed line in each plot represents the nominal homopause for the model (this is the CO_2 homopause). There is a significant altitude range over which particles from most species originate. Note that the altitudes of the various epochs are not directly comparable, since the density profiles are significantly different. A better measure is to look at the distribution relative to the homopause.

The mean escape altitude for each species is shown in Table 3. This is actually calculated directly by the model and does not use the binned data. The lower part of the table contains the mean altitude for specific elements obtained calculating a weighted mean based on the yield of each species where that element escapes.

In addition to the model runs with the expected parameters, a series of cases were run where the initial conditions or other input parameters were varied to determine the model sensitivity. All of the studies were based on the 1 EUV results. In all cases, both the actual value and the percent change from the standard 1 EUV case are shown. The sensitivity studies can be grouped into four sets, each studying a different type of parameter. The first set varies the parameters of the impacting ion. The second set modified the target atmosphere. The third changed the collision cross sections, and the final set varied the scattering functions. For each component of the model that was changed, a case with an increase and one with a decrease were run. The behavior for each case in a pair were similar but with opposite signs and for simplicity, only one of the pair will be discussed—the other would have the same comments with the opposite sign for all effects.

The first study (see Tables 4–6) modified the parameters of the impacting O^+ ion. Four model runs were performed. In the first two, the initial energy was increased and decreased

by 25% (to 1250 eV and 750 eV). As expected, increasing the energy increases the yields, but the increases are generally $\sim$ 20%. This is less than the percent change in the initial energy primarily because the energy spectrum of the escaping particles, as represented by the fraction of the energy in the escaping particles, is shifted to higher energies. Thus instead of all the extra energy being used to increase the yield, part of it is being used to increase the mean escape energy. While counter-intuitive, the source altitude for the O increases slightly at higher energies. Particles from the exobase zone on escape trajectories occasionally have collisions well above that level as they escape (see the upper tails in figure 7). Due to the forward nature of collisions, the escape of the resulting particles is primarily controlled by the available energy. With the increased energy of upwardly directed particles, more of these high altitude collisions lead to multiple escaping particles. The enhancement in this region is then sufficient to increase the mean escape altitude. In the second pair of experiments, the initial angle was changed by 15°. When it was made shallower (about half way between the expected angle and tangent to the atmosphere), the yields increased due to the smaller change in angle required for the particles to have upward motion. The increased yield is also reflected in an increased amount of the initial energy in escaping particles. The relatively large energy increase, compared to the yield, is due to an increase in the particles that scatter out of the atmosphere after the first collision, carrying a significant fraction of their initial energy with them. As expected with a more shallow impact angle, the initial (and many subsequent) collisions occurred at higher altitudes, raising the source altitude for the escaping particles.

The second study (see Tables 7–9) modified the model atmosphere by changing the number density of the various species. While the resulting atmospheres are unphysical, they are useful for comparison to the original one. In the first two cases, Ar, a minor gas in the atmosphere, was modified by 25%. The only significant change from the standard case is about a 25% change in the Ar yield. The large change in N_2 in the "Low Ar" case

is probably not meaningful, but is just statistical noise–it is at the 2 σ level. In the next two cases, the number density of CO_2, the major constituent at the exobase altitude, was changed by 25%. In general, most of the changes are small. The changes in N (from N_2 dissociation) and Ar yields are due to the significant increase in their mixing ratios (as minor species) with the decrease in CO_2 abundance. The changes in the source altitudes are due to the changes in the pressure caused by the change in CO_2. The final set of changes were to O, the dominant species in the exosphere. Much like the changes to CO_2, the net effect was small. Since the immediate source of escaping O is primarily CO_2, the change has little effect on the total O loss. The primary effect is to reduce the probability of thermalizing an escaping particle with a high altitude impact or other energy loss. This tends to result in slightly higher yields and escape energies for the "Low O" case.

The third study (see Tables 10–12) involved changing the collisional cross section of the species for all its collisions. First, the cross section of Ar, a minor constituent, was changed by 25% (in self collision cases, the cross section of each atom was changed by 25% for a net decrease of 43.75% and an increase of 56.25%). The general effect of the larger cross sections was to slightly enhance the yield of Ar. Although difficult to measure due to uncertainty, there may have been a broader effect of shortening the distances between collisions which reduces the amount of electronic excitation. In the other cases, the cross section of O, one of the major gases (at least as far as the number of collisions) was changed by 25%. The increase in cross section created a significant increase in the yield of most species. Since many of the particles involved in the collision cascades are O, primarily from dissociated CO_2, the change in cross sections affected many of the particles. With a larger O cross section, the distance to the next momentum transferring collision was reduced, reducing the energy loss due to electronic transfer. The net effect is to have more energy available for escaping particles, enhancing all yields.

The final study (see Tables 13–15) was to modify the scattering functions for selected collisions. In the first case, "Forward Ar," the Henyey-Greenstein parameter (see Equation A2 in the Appendix) for the cross section for all collisions involving Ar was changed from 0.5 to 0.75, causing the scattering to be more forward. In the second case, the parameter was changed to 0.25. In general, there was little change in the results. The only exception was a possible enhancement of the Ar yield when its scattering is less forward. In the two cases where the scattering of CO_2 was changed, this involved changing the scattering angle of the particle with the C atom in collisions between CO_2 and O—these are the most important ones. All of the parameters were changed by either 0.25 or halfway to ± 1.0, if that was a smaller value. Each case was changed by the same amount for the two trials. In these cases, most of the changes are only marginally significant compared to the numerical noise of the model. It does appear that making the scattering more forward generally increases the yield, and thus the escaping energy. This may be due to the forward direction of the CO fragment in early collisions creating more upward moving fast O atoms that can eject particles on their way out. This is slightly supported by the last two cases where the scattering angle of the O fragments from the O + CO_2 collisions was modified in a similar way. But, in this case there doesn't seem to be any statistical significance to most of the changes.

5. Discussion

In order to obtain the actual fluxes of particles escaping Mars, it is necessary to multiply the yields by the total impacting flux. The plasma modeling results of Luhmann *et al.* (1992) indicate impacting fluxes of O^+ ions of 2.6×10^9 cm^{-2} s^{-1} at 6 EUV, 1.6×10^8 cm^{-2} s^{-1} at 3 EUV and 4.8×10^5 cm^{-2} s^{-1} at 1 EUV. Using these fluxes and the model yields gives the loss fluxes indicated in Table 16. The table also includes estimates for the

two other major loss processes for O atoms (Luhmann *et al.* 1992) and the net water loss rate obtained by combining the three oxygen loss processes after removing enough O to account for the loss of CO_2.

By taking the loss fluxes (Figure 8) and integrating over time, it is possible to estimate the total amount of atmosphere lost from Mars over the last 3.5 Gyr. Doing this yields a loss of $\sim$0.8 bars of CO_2 and a loss equivalent to a $\sim$50 m thick layer of water covering the planet.

While the 50 m of water is less than the geological estimates (Carr 1996), it is still an increase over previous estimates of 9 m (Yung *et al.* 1988; Kass and Yung 1999). Furthermore, it is quite likely that some of the water is still stored in the planet. The 0.8 bars of CO_2 probably represent sufficient CO_2 to enhance the atmospheric greenhouse and warm the surface. It is also a significant increase over the estimate of 0.14 bars by Luhmann *et al.* (1992). In this case, both estimates use the same impacting fluxes, but differ in the model calculation of the sputtering yield. The Monte-Carlo model improves the previous work by always treating CO_2 as a molecule and allowing it to dissociate. First, this allows the energetic O to impact any of the three atoms and transfer momentum to the entire molecule. Secondly, the dissociation during the full cascade creates many CO and C fragments that can escape. The fragments need less energy to escape since they are light, and more importantly, have smaller cross sections and thus will travel further before colliding again. This allows deeper collisions to potentially create particles capable of escaping. The actual difference in source altitudes for escaping CO_2, CO, and C reflects more than this effect (see Table 3). It is also caused by the energy the particle has after being accelerated and the number of collisions it can undergo and still escape. CO_2 usually has much less energy since larger energy transfers result in dissociation.

There are several improvements in this Monte-Carlo model over the previous one (Kass

and Yung 1995). In particular, the current model addresses the issues raised by Johnson and Liu (1998) by using the updated cross sections and scattering functions from their work. Three changes account for most of the differences in the results. First, the model now incorporates energy loss due to electronic excitation. Secondly, the model does not assume that CO_2 always dissociates fully. And finally, it uses many improved cross sections and scattering functions from molecular dynamical calculations. Of the three effects, allowing CO_2 to partly dissociate causes most of the reduction from the original estimate of ~ 3 bars of CO_2 lost to the current result of ~ 0.8 bars lost. The changes in the cross sections and especially the scattering function caused most of the change between the original estimate of ~ 80 m of water lost and the current ~ 50 m lost. While these results are closer to the original calculations by Luhmann *et al.* (1992), the two results are still very different. This is primarily because the original calculations simplified the treatment of CO_2, but is also due to the better cross sections and scattering functions that have been calculated since then and incorporated into the current model.

The model indicates that the average energy per escaping atom is ~ 25 eV for the 6 EUV and 3 EUV atmosphere. For the 1 EUV case, the average energy is ~ 21 eV. Part of this difference is the effect of the H_2 in the present atmosphere which acts as an energy sink since it is too light to effectively transfer momentum to anything else. It is not a large sink and thus there was no attempt to put H_2 in the past atmospheres. Some experiments in doing so indicated that it has about a 5% effect on the yield.

Since the mean escape energies are much higher than the minimum escape energy for the atmospheric species involved, the sputtering process does not directly fractionate the atmosphere. With over 20 eV of energy, the mass difference between the various isotopes will not have a noticeable effect. While the sputtering process itself does not fractionate, most of the escaping molecules come from above the homopause. Because of this, the

isotopic composition of the source region differs from the bulk atmosphere (since the heavier isotopes will have a smaller scale height than the lighter ones). The net result is that atmosphere lost by sputtering does fractionate the bulk atmosphere.

There are three sources of error in the calculation of the total amount of atmosphere lost: the error in the Monte-Carlo model, the error in the model parameters and the error in the calculation of the impacting fluxes. Being a fast Monte-Carlo model, it was run a sufficient number of times to make the inherent model error small, but the statistical uncertainty depends on the parameter being studied. The most uncertain quantities are the yields for CO_2, N_2 and Ar, but even these values appear to be good to $\lesssim 7\%$ and and most of the quantities are accurate at about the 1% level. The high numerical uncertainty in CO_2 yield does not significantly impact the derived results since most of the carbon and oxygen escape as other species whose contributions overwhelm the uncertainty in CO_2.

The sensitivity studies were performed to help quantify the effects of the errors in the model parameters. This includes the model atmospheres, the cross sections, the scattering functions and the initial conditions. Only the results for a given minor species are sensitive to that species' parameters. The major species (CO_2 and O and their fragments) will affect all the results. The sensitivity studies do show that most of the effects of moderate changes to the major species generally result small (and often statistically insignificant) changes. Combined with the fact that most of the important cross sections and scattering functions are now derived from molecular dynamical calculations or laboratory experiments and should be accurate, the model results appear to be quite robust. Even if the compositions of the ancient atmospheres are inaccurate, there seems to be a negative feedback procedure in the model that makes the results fairly insensitive to the overall atmospheric composition. Thus while the absolute altitude for the exobase may vary, its altitude relative to the homopause should be constant, as will be the yields for the various atoms. The largest

source of error in the Monte-Carlo model results is probably the parameters of the impacting O^+ ions, especially since they have the largest relative impact on the final results. Even in these cases, the relative change in model results is generally smaller than the relative change of the initial parameters. Overall, we estimate that the model results are valid to within 50%.

The final source of error is in the calculation of the magnitude of the impacting ion flux. Unfortunately, the calculations of the impacting fluxes are based on models of the young sun and its solar wind (Zhanle and Walker 1982). Because of this, they are much less certain and may have errors as large as an order of magnitude. Thus the estimates for the total losses are probably only good to within a factor of ten.

Sputtering, by the process modeled here, only occurs on planets with small or no intrinsic magnetic fields. A dipole moment $\gtrsim$ 0.5% the terrestrial field is sufficient to prevent the solar wind from interacting with the planet's ionosphere and sputtering will not occur (Hutchins *et al.* 1997). During the early history of Mars, there is evidence for a strong magnetic field (Acuña *et al.* 1998; Stevenson *et al.* 1983; Kieffer *et al.* 1992). If this field existed during the early part of the sputtering history being considered here, it would have stopped much of the sputtering (Hutchins *et al.* 1997). Sputtering could still have occurred during field reversals or other periods when the field was weaker or did not exist. It has also occurred since the field disappeared. Thus while a magnetic field may have kept sputtering from removing the full $\sim$ 0.8 bars of CO_2, sputtering has still played a role in the evolution of the Martian atmosphere.

6. Conclusion

The Monte-Carlo model results indicate that Mars has lost $\sim$ 0.8 bars of CO_2 and $\sim$ 50 m of water over the last 3.5 Gyr. This implies extensive evolution of the atmosphere over time. The CO_2 represents most, if not all, of the CO_2 needed to warm Mars sufficiently to allow for liquid water near the surface. Both the water and the CO_2 are large volumes compared to the known reservoirs on the planet. The model results indicate that sputtering is a significant process in the evolution of the atmosphere of Mars.

We estimate that the Monte-Carlo model results have an uncertainty of 50%. This is based on the sensitivity studies and our estimates of the quality of the input data. Unfortunately, the uncertainty in the impacting flux, which is used for the temporal integration, is much larger, and probably dominate the total error.

Because most of the major sputtering occurred early in the history of Mars, it is difficult to test the model results. In-situ measurements of the modern escape fluxes of heavier species from Mars would help to constrain at least the value for the present epoch and verify the validity of the sputtering model itself. This is especially the case for C, because sputtering appears to be its dominant escape mechanism (for O, the other escape mechanisms will overwhelm the contribution from sputtering).

A. Numerical Model Description

While the Monte-Carlo model itself is fairly simple, the complexity is introduced by the need to model multibody collisions involving dissociation and non-isotropic scattering. In part due to the simplicity of the method, one of the most important factors in producing meaningful results is the use of correct parameterizations and values for the necessary input parameters. Thus the description of the model involves two aspects. The first is the

actual processing that the model performs and the second are the parameters defining the behavior of the atoms and molecules it is modeling (Kass 1999).

For each numerical experiment, the model calculates the collision cascade for 10,000 ions with an impact angle of $\sim 124°$ and an energy of 1 keV, the mean parameters derived by Luhmann and Kozyra (1991) for O^+ ions impacting the upper atmosphere of Mars. For each impacting ion, the model determines the altitude and target of its first collision. After resolving that collision, it puts all of the resulting particles in a queue. The model then pulls each particle out of the queue one at a time and has it collide with its next target. The results are again put back into the queue. If a particle reaches the top of the model atmosphere ($\sim$500 km) with sufficient energy to escape the planet, it is counted as an escaped particle. If it does not have enough energy, the particle is counted as being on a ballistic trajectory and is ignored. Particles that have less than 1.5 eV are also removed from the calculation. They have too little energy to cause an atom of interest in the model to escape, and their removal significantly speeds up the model execution. Their energy is assumed to eventually become thermal energy in the upper atmosphere. The calculation of a collision and the storing of its products continues until the queue is empty. At that point, all the statistics for that impacting particle are tallied and the next particle is started.

For each particle's flight and collision(s), the process is divided into two parameterized steps. The first step determines where the collision occurs and what molecule or atom is the target. Then a second step determines the results of the collision. The important part of the results are the direction and kinetic energy of each particle (atom or molecule) resulting from the collision.

In determining the location and target for the next collision, the model uses a table of energy dependent cross sections. Each cross section (see Figures 9 through 11) measures the effective area of each atom or molecule in the atmosphere. The cross sections depend on

the two species potentially involved in the collision as well as the energy of the impacting particle. The energies are measured in the atmospheric frame of reference. For the case of two atoms colliding, the cross section is a single value (depending on the energy) and if the moving atom passes within the given area surrounding the target atom, they collide. For poly-atomic species, the cross section is a bit more complex (for example, Figure 10) since the molecule can dissociate, and possibly do so in multiple patterns. There is a total cross section (the solid line) representing the area where some type of collision between the two species will occur. This is then broken into individual cross sections for each possible dissociation path. Thus CO_2 can dissociate into CO + O or into C + 2O, and each possibility has its own cross section. The case where the CO_2 does not dissociate is the remainder when all the dissociation paths are subtracted from the total cross section. The cross sections used in the model come from many different sources. The O + O, O + N_2, and N_2 + N_2 cross sections are from Ishimoto *et al.* (1986). The O + H cross section at low energies from Hodges (1993) was extrapolated out to 1 keV. O + O^+ and O + H^+ cross sections are from Stebbings *et al.* (1964). The cross sections for H + H^+ came from an extrapolation of the literature survey of Smith and Bewtra (1978). Many of the ones involving CO_2 (O + CO_2, O + CO, CO + CO_2 and CO_2 + CO_2), which are among the most important cross sections to the model, are from molecular dynamical calculations by Johnson and Liu (1998). Finally, where no experimental or laboratory values were available, the cross section was calculated by taking the molecular and atomic radii of the species (Forsythe 1954; Kaye and Laby 1995) and using $4\pi(r_a + r_b)^2$, where r_a and r_b are the radii of the two species involved. For cases where one of the species can dissociate, it was assumed to dissociate as long as the center of mass energy exceeded the dissociation energy. Excluding CO, the current set of cross sections do not produce fast poly-atomic species, and thus many collisions involving fast poly-atomic moving particles are ignored (for example, there is no case for N_2 + N_2 at high energies).

The model determines the species of the target, and the location by first randomly choosing the path length until the next collision ($\tau = -\log(rnd)$ where $0 < rnd < 1$ is a random number).

$$\tau = l \sum_{\text{species}} N_i \sigma_i(e) \tag{A1}$$

where l is the distance and N_i and $\sigma_i(e)$ are the the local number density and energy dependent total cross section for species i, respectively. This allows the actual location of the collision to be calculated, using the integrated cross section for each layer in the model atmosphere. If the particle exits the the top of the top layer of the model atmosphere, it is assumed to be on a free trajectory and either escapes or thermalizes (depending on whether or not it has sufficient energy to escape). As the particle travels through the atmosphere, it looses energy by exciting the surrounding atmosphere. The energy lost is calculated using the curves from Johnson and Liu (1998) (see their Figure 6, curves for S_e^{O} and $S_e^{\mathrm{CO_2}}$). Once the model knows where the collision occurs, it determines the species of the target. This is done by randomly selecting a target species and a resulting set of particles, each possibility weighted by its cross section and number density.

Once the location and target species (along with the resulting particles) for the collision have been determined, the model determines the energy and direction of each resulting particle. This is controlled by the conservation of momentum and energy (after subtracting any lost due to dissociation) and the scattering function for each resulting particle. The latter are described in terms of two angles. The first is the azimuthal angle (ϕ, between 0 and 2π), the rotation around the direction of the incident particle. By symmetry, ϕ is assumed to be isotropic. The second is the phase angle (θ or χ in the CM frame), the angle between the direction of the incident particle and that and the resulting particle. The probabilistic function for χ depends on the species involved in the collision and the specific fragment in question. For computational simplicity, the phase functions are expressed as

Henyey–Greenstein (HG) functions:

$$hg(g,\chi) = 0.5\left(\frac{1-g^2}{1+g^2-2g\cos(\chi)}\right) \tag{A2}$$

where $-1 < g < 1$ is the parameter defining the type of scattering. Negative values represent backscattering (at least in the CM frame); positive ones are forward scattering and zero indicates isotropic scattering. In order to improve some of the scattering functions used, they were fitted with double Henyey–Greenstein functions (Goody and Yung 1989):

$$dhg(a,g_1,g_2,\chi) = a\,hg(g_1,\chi) + (1-a)\,hg(g_2,\chi) \tag{A3}$$

with three parameters. Many of the values used in the model (Table 17) come from Johnson and Liu (1998) (and personal communication). The curves for O + O come from Johnson *et al.* (1999). The curve for O + H comes from Gurwell and Yung (1993). All of the cases not listed are either single HG functions with $g = 0.5$ for collisions without dissociation or isotropic for cases with dissociation.

For each collision, the result is determined by solving the conservation equations. Since these are under-determined, a sufficient number of scattering angles are determined randomly, using the appropriate distribution functions. Because of the representation used for collisions, they are classified based on the number of resulting particles (there will always be two initial particles, the impactor and the target). For collisions resulting in two particles (i.e., neither dissociates), only two angles are needed. Furthermore, the collision can be performed in a plane (the one containing both outgoing particles). Thus in this case, the first angle is the phase angle of the impacting particle. The second angle is the azimuthal angle of the collision plane. In a collision that results in three particles, five angles are needed. For simplicity, the model randomly determines all three azimuthal angles and the phase angle for two of the fragments. Usually they are the two fragments from the target (if an impacting CO dissociates, the fragment whose phase angle is determined is

random). In the case where the collision results in four particles, the phase and azimuthal angles for each particle are determined randomly. In cases resulting in five particles (which can only occur in the model when CO impacts CO_2 and both dissociate completely), both angles are determined for each fragment. In addition, the energy of one C atom is selected using the probability distribution from Johnson and Liu (1998). In this case the equations are quadratic and may occasionally need to be calculated with several sets of random parameters to actually get a physical solution.

Once the model uses the random variables and the conservation laws to calculate the velocity of each fragment in the CM frame, each particle's velocity is transformed into the atmospheric frame and the energy and direction of the particle is stored. Each particle is evaluated to determine if it can still have an effect (i.e., has enough energy to either escape or allow another atom to escape). Those that are still relevant are stored in the queue of particles to be processed.

As each cascade is finished, the statistics (number of particles escaping as well as source location) are stored. Once all 10,000 incident ions have been run, the model determines the total yield for each species (and fragment). One advantage of using the Monte-Carlo model with the parameterizations is that it runs very fast. This allows the model to run enough particle to gather meaningful statistics on the yields of even trace atmospheric species. It also has the advantage of making the model flexible and allowing it to gather statistics on other relevant quantities (although, some quantities will require more particles to insure a sufficiently large statistical sample). The model also allows one to look at the actual effects of the various processes and determine what are the important processes.

We thank R. E. Johnson for many valuable discussions on the Monte Carlo code and M. Gerstell for helpful comments on the manuscript. This research was supported in part by NASA grants NAG5-4022 and AST-9816409 to the Califorina Institute of Technology.

DMK acknowledges the support of an NSF Fellowship while a graduate student at Caltech.

REFERENCES

Acuña, M. H., J. E. P. Connerney, P. Wasilwski, R. P. Lin, K. A. Anderson, C. W. Carlson, J. McFadden, D. W. Curtis, D. Mitchell, H. Reme, C. Mazelle, J. A. Sauvaud, C. d'Uston, A. Cros, J. L. Medale, S. J. Bauer, P. Cloutier, M. Mayhew, D. Winterhalter, N. F. Ness 1998. Magnetic Field and Plasma Observations at Mars: Initial Results of the Mars Global Surveyor Mission, *Science,* **279**, 1676-1680.

Carr, M. H. 1996. *Water on Mars,* Oxford University Press, New York.

Fanale, F. P., J. R. Salvail, W. B. Banerdt, R. S. Saunders 1982. Mars—the Regolith-Atmosphere-Cap System and Climate Change *Icarus,* **50**, 381-407.

Forget, F., R. T. Pierrehumbert 1997. Warming Early Mars with Carbon Dioxide Clouds that Scatter Infrared Radiation, *Science,* **278**, 1273-1276.

Forsythe, W. E. 1954. Smithsonian Physical Tables, *Smithson. Misc. Collect.,* **120**, *Publ. 4169*, Smithson. Inst., Washington D.C.

Goody, R. M., Y. L. Yung 1989. *Atmospheric Radiation Theoretical Basis,* 2^{nd} ed., Oxford University Press, New York.

Gurwell, M. A., Y. L. Yung 1993. Fractionation of Hydrogen and Deuterium on Venus due to Collisional Ejection, *Planet. Space Sci.,* **41**, 91-104.

Haberle, R. M. 1998. Early Mars Climate Models, *J. Geophys. Res.,* **103**, 28467-28479.

Hodges Jr., R. R. 1993. Isotopic Fractionation of Hydrogen in Planetary Exospeheres due to Ionosphere-Exosphere Coupling—Implications for Venus, *J. Geophys. Res.,* **98**, 10833-10838.

Hunten, D. M. 1993. Atmospheric Evolution of the Terrestrial Planets, *Science,* **259**, 915-920.

Hutchins, K. S., B. M. Jakosky, J. G. Luhmann 1997. Impact of a Paleomagnetic Field on Sputtering Loss of Martian Atmospheric Argon and Neon, *J. Geophys. Res.,* **102**, 9183-9189.

Ishimoto, M., M. R. Torr, P. G. Richards, D. G. Torr 1986. The Role of Energetic O^+ Precipitation in a Midlatitude Aurora, *J. Geophys. Res.,* **91**, 5793-5802.

Jakosky, B. M. 1991. Mars Volatile Evolution—Evidence from Stable Isotopes, *Icarus,* **94**, 14-31.

Johnson, R. E., D. Schellemberger, M. Wong 1999. The Sputtering of an Oxygen Thermosphere by Energetic O^+, *Planet. Space Sci.,* submitted.

Johnson, R. E., M. Liu 1998. Sputtering of the Atmosphere of Mars 1. Collisional Dissociation of CO_2, *J. Geophys. Res.,* **103**, 3639-3647.

Johnson, R. E., J. G. Luhmann 1998. Sputtering Contribution to the Atmospheric Corona on Mars, *J. Geophys. Res.,* **103**, 2649-3653.

Johnson, R. E. 1990. *Energetic Charged-Particle Interactions with Atmospheres and Surfaces,* Springer–Verlag, New York.

Kass, D. M. 1999. *Change in the Martian Atmosphere,* Ph. D. thesis, California Institute of Technology.

Kass, D. M., Y. L. Yung 1999. Water on Mars: Isotopic Constraints on Exchange Between the Atmosphere and Surface, *Geophys. Res. Lett.,* **26**, 3653-3656.

Kass, D. M., Y. L. Yung 1995. Loss of Atmosphere from Mars due to Solar Wind–Induced Sputtering, *Science,* **268**, 697-699.

Kasting J. F. 1991. CO_2 Condensation and the Climate of Early Mars, *Icarus,* **94**, 1-13.

Kaye, G. W. C., T. H. Laby 1995. *Tables of Physical and Chemical Constants*, Longman, New York.

Kieffer, H. H., B. M. Jakosky, C. W. Snyder, M. S. Matthews (Eds.) 1992, *Mars,* The University of Arizona, Tucson.

Luhmann, J. G., R. E. Johnson, M. H. G. Zhang 1992. Evolutionary Impact of Sputtering of the Martian Atmosphere by O^+ Pickup Ions, *Geophys. Res. Lett.,* **19**, 2151-2154.

Luhmann, J. G., J. U. Kozyra 1991. Dayside Pickup Oxygen Ion Precipitation at Venus and Mars—Spatial Distributions, Energy Deposition, and Consequences, *J. Geophys. Res.,* **96**, 5457-5467.

McElroy, M. B. 1972. Mars: An Evolving Atmosphere, *Science,* **175**, 443-445.

McElroy, M. B., T. Y. Kong, Y. T. Yung 1977. Photochemistry and Evolution of Mars' Atmosphere: A Viking Perspective, *J. Geophys. Res.,* **82**, 4379-4388.

McKay C. P., W. L. Davis 1991. Duration of Liquid Water Habitats on Early Mars, *Icarus,* **90**, 214-221.

Nair, H., M. Allen, A. D. Anbar, Y. L. Yung, R. T. Clancy 1994. A Photochemical Model of the Martian Atmosphere, *Icarus,* **111**, 124-150.

Pollack, J. B., J. F. Kasting, S. M. Richardson, K. Poliakoff 1987. The Case for a Wet, Warm Climate on Early Mars, *Icarus,* **71**, 203-224.

Smith, P. H., N. K. Bewtra 1978. Charge Exchange Lifetimes for Ring Current Ions, *Space Sci. Rev.,* **22**, 301-317.

Shizgal, B. D., G. G. Arkos 1996. Nonthermal Escape of the Atmospheres of Venus, Earth and Mars, *Rev. Geophys.,* **34**, 483-505.

Stebbings, R. F., A. C. H. Smith, H. Ehrhardt 1964. Charge Transfer between Oxygen Atoms and O^+ and H^+ Ions, *J. Geophys. Res.,* **69**, 2349-2355.

Stevenson, D. J., T. Spohn, G. Schubert 1983. Magnetism and Thermal Evolution of the Terrestrial Planets, *Icarus,* **54**, 466-489.

Tombrello, T. A. 1982. Solar System Sputtering, *Radiation Effects,* **65**, 149-158.

Watson, C. C. 1980. *Topics in Classical Kinetic Transport Theory with Applications to the Sputtering and Sputter–Induced Mass Fractionation of Solid Surfaces and Planetary Atmospheres*, Ph.D. Thesis, Yale University.

Yung, Y. L., J. S. Wen, J. P. Pinto, M. Allen, K. K. Pierce, S. Paulson 1988. HDO in the Martian Atmosphere: Implications for the Abundance of Crustal Water, *Icarus,* **76**, 146-159.

Zhang, M. H. G., J. G. Luhmann, S. W. Bougher, A. F. Nagy 1993. The Ancient Oxygen Exosphere of Mars—Implications for Atmosphere Evolution, *J. Geophys. Res.,* **98**, 10915-10923.

Zhanle, K. J., J. C. G. Walker 1982. The Evolution of Solar Ultraviolet Luminosity, *Rev. Geophys.,* **20**, 280-292.

This manuscript was prepared with the AAS LaTeX macros v5.0.

Table 1. Model Yields for Each Atmosphere

Species	Atmosphere			
	6 EUV	3 EUV	1 EUV	Pure O
O	4.63	4.71	5.943 ±0.025	2.41
CO_2	0.03	0.04	0.030 ±0.002	···
CO	0.80	0.93	0.462 ±0.006	···
C	0.32	0.43	1.461 ±0.014	···
N_2	···	···	0.018 ±0.001	···
N	···	···	1.099 ±0.013	···
Ar	···	···	0.058 ±0.003	···
Total O	5.49	5.72	6.465 ±0.026	2.41
Total C	1.15	1.40	1.953 ±0.015	···
Total N	···	···	1.136 ±0.013	···
Total Yield	6.64	7.12	9.611 ±0.043	2.41

Note. — The yield (number ejected per incident ion) for each species in the four atmospheres used. Blank entries indicate species that were not in the model atmosphere. The "Total" lines represent the total number of the given atom that are sputtered. The last line is the total number of atoms ejected by each incident ion. The fourth atmosphere is not realistic but is used for comparisons.

Table 2. Model Energy Distribution

Energy	Atmosphere		
Sink	6 EUV	3 EUV	1 EUV
Electronic	580	565	401.6 ±0.9
Dissociation	152	158	252.1 ±0.5
Thermal	102	101	146.2 ±0.2
Escaping	166	176	200.1 ±1.0

Note. — Ultimate location of the ion's initial keV of energy. These are the mean values for all the particles run in the model. "Electronic" refers to loss to electronic excitation; "Dissociation" is energy used to dissociate atmospheric molecules. "Thermal" is kinetic energy no longer sufficient to allow particles to escape—it also includes particles on ballistic trajectories. "Escaping" is the total energy of the particles that leave Mars. All energies are in eV.

Table 3. Mean Source Altitude for Sputtering

Species	Atmosphere		
	6 EUV	3 EUV	1 EUV
O	206	180	159.4 ±0.2
CO_2	248	218	191.1 ±0.9
CO	211	191	178.2 ±0.3
C	224	200	181.3 ±0.2
N_2	...	...	204.6 ±1.8
N	...	...	192.2 ±0.3
Ar	...	...	192.1 ±0.8
Mean O	207	182	161.0 ±0.2
Mean C	215	195	180.7 ±0.2
Mean N	...	...	192.6 ±0.4

Note. — The mean altitude that each species is lost from. The last three lines contain the mean altitude that each type of atom is lost from. These are calculated using weighted averages based on the yields. All altitudes are in km.

Table 4. Model Yields for Different Input Parameters

Species	Input Parameter Varied				
	1 EUV	1250 eV	750 eV	−15°	+15°
O	5.94	7.18 (21%)	4.67 (−21%)	6.88 (16%)	5.31 (−11%)
CO_2	0.03	0.04 (29%)	0.02 (−24%)	0.04 (42%)	0.02 (−20%)
CO	0.46	0.56 (21%)	0.36 (−23%)	0.56 (22%)	0.41 (−12%)
C	1.46	1.75 (20%)	1.17 (−20%)	1.89 (30%)	1.25 (−15%)
N_2	0.02	0.02 (30%)	0.01 (−25%)	0.03 (54%)	0.02 (−16%)
N	1.10	1.32 (20%)	0.89 (−19%)	1.52 (38%)	0.91 (−17%)
Ar	0.06	0.08 (31%)	0.04 (−25%)	0.10 (69%)	0.04 (−31%)
Total O	6.47	7.81 (21%)	5.07 (−22%)	7.53 (16%)	5.76 (−11%)
Total C	1.95	2.34 (20%)	1.55 (−21%)	2.50 (28%)	1.68 (−14%)
Total N	1.14	1.36 (20%)	0.92 (−19%)	1.58 (39%)	0.94 (−17%)
Total Yield	9.61	11.6 (21%)	7.58 (−21%)	11.7 (22%)	8.42 (−12%)

Note. — The yield for each species as the initial state of the impacting O^+ ion changes. The percentage changes are relative to the 1 EUV atmosphere (shown in first column, from Table 1). In two cases, the initial energy is changed by 25%. In the other two cases, the initial angle when it enters the atmosphere is changed by 15°.

Table 5. Model Energy Distribution for Different Input Parameters

Energy	Input Parameter Varied				
Sink	1 EUV	1250 eV	750 eV	−15°	+15°
Electronic	402	500 (25%)	302 (−25%)	360 (−10%)	425 (+5%)
Dissociation	252	310 (23%)	193 (−24%)	246 (−2%)	253 (0%)
Thermal	146	180 (23%)	112 (−23%)	138 (−5%)	149 (+2%)
Escaping	200	260 (30%)	143 (−29%)	256 (+28%)	173 (−13%)

Note. — Ultimate location of the ion's initial keV of energy as the initial state of the impacting O^+ ion changes. The percentage changes are relative to the 1 EUV atmosphere (shown in first column, from Table 2). In the first two cases, the initial energy is changed by 25%. In the other two cases, the initial angle when it enters the atmosphere is changed by 15°. All energies are in eV.

Table 6. Mean Source Altitude for Different Input Parameters

Species	Initial Condition Varied				
	1 EUV	1250 eV	750 eV	−15°	+15°
O	159	161 (+1.2%)	156 (−2.4%)	166 (4.1%)	155 (−2.6%)
CO_2	191	189 (−0.9%)	189 (−1.0%)	192 (0.6%)	191 (−0.3%)
CO	178	178 (0%)	179 (+0.3%)	181 (1.8%)	177 (−0.9%)
C	181	181 (−0.4%)	182 (+0.4%)	186 (2.6%)	179 (−1.5%)
N_2	205	206 (+0.8%)	203 (−0.7%)	205 (0.0%)	203 (−0.6%)
N	192	191 (−0.6%)	193 (+0.5%)	196 (2.1%)	190 (−1.1%)
Ar	192	192 (+0.1%)	195 (+1.5%)	192 (0.2%)	193 (+0.3%)
Mean O	161	163 (+1.1%)	158 (−2.2%)	167 (4.0%)	157 (−2.4%)
Mean C	181	180 (−0.3%)	181 (+0.3%)	185 (2.4%)	178 (−1.4%)
Mean N	193	192 (−0.6%)	193 (+0.4%)	197 (2.1%)	190 (−1.1%)

Note. — The mean altitude that each species is lost from as the initial state of the impacting O^+ ion changes. The percentage changes are relative to the 1 EUV atmosphere (shown in first column, from Table 3). In two cases, the initial energy is changed by 25%. In the other two cases, the initial angle when it enters the atmosphere is changed by 15°. All altitudes are in km.

Table 7. Model Yields for Modified Atmospheres

Species	Species Modified						
	1 EUV	Low Ar	High Ar	Low CO_2	High CO_2	Low O	High O
O	5.94	5.97 (+0.4%)	5.93 (−0.3%)	5.95 (+0.1%)	5.86 (−1.3%)	5.98 (+0.9%)	5.87 (−1.3%)
CO_2	0.03	0.03 (−1.3%)	0.03 (−3.0%)	0.03 (−7.7%)	0.04 (+24.1%)	0.03 (−4.7%)	0.03 (+3.7%)
CO	0.46	0.46 (−0.1%)	0.45 (−2.5%)	0.40 (−13.7%)	0.51 (+11.3%)	0.46 (−0.4%)	0.47 (+1.2%)
C	1.46	1.46 (−0.2%)	1.46 (+0.2%)	1.52 (+3.7%)	1.42 (−3.1%)	1.52 (+4.3%)	1.43 (−2.3%)
N_2	0.02	0.02 (−12.0%)	0.02 (−3.8%)	0.02 (+2.7%)	0.02 (−2.7%)	0.02 (+2.7%)	0.02 (−3.8%)
N	1.10	1.10 (+0.5%)	1.09 (−1.2%)	1.28 (+16.0%)	0.97 (−11.7%)	1.11 (+1.3%)	1.08 (−1.6%)
Ar	0.06	0.04 (−24.3%)	0.07 (+22.1%)	0.06 (+11.3%)	0.05 (−11.5%)	0.06 (+1.9%)	0.05 (−5.2%)
Total O	6.47	6.49 (+0.4%)	6.44 (−0.5%)	6.40 (−0.9%)	6.45 (−0.2%)	6.51 (+0.8%)	6.40 (−1.1%)
Total C	1.95	1.95 (−0.2%)	1.94 (−0.5%)	1.94 (−0.6%)	1.97 (+0.7%)	2.01 (+3.0%)	1.93 (−1.4%)
Total N	1.14	1.14 (0%)	1.12 (−1.3%)	1.31 (+15.5%)	1.01 (−11.4%)	1.15 (+1.3%)	1.12 (−1.7%)
Total Yield	9.61	9.62 (+0.1%)	9.57 (−0.4%)	9.72 (+1.2%)	9.48 (−1.4%)	9.74 (+1.3%)	9.49 (−1.2%)

Note. — The yield for each species as the model atmosphere was varied. In all cases, the indicated species was changed by 25%. The percentage changes are relative to the 1 EUV atmosphere (shown in first column, from Table 1).

Table 8. Model Energy Distribution for Modified Atmospheres

Energy Sink	Species Modified						
	1 EUV	Low Ar	High Ar	Low CO_2	High CO_2	Low O	High O
Electronic	402	403 (+0.4%)	400 (−0.4%)	389 (−3.1%)	412 (+2.6%)	398 (−1.0%)	405 (+0.9%)
Dissociation	252	251 (−0.2%)	252 (+0.1%)	262 (+4.1%)	245 (−3.0%)	253 (+0.5%)	251 (−0.5%)
Thermal	146	144 (−1.7%)	149 (+1.7%)	152 (+3.8%)	142 (−2.6%)	146 (−0.3%)	146 (+0.1%)
Escaping	200	202 (+0.8%)	199 (−0.5%)	197 (−1.7%)	201 (+0.4%)	203 (+1.6%)	198 (−1.1%)

Note. — Ultimate location of the ion's initial keV of energy as the model atmosphere is modified. In all cases, the indicated species was changed by 25%. The percentage changes are relative to the 1 EUV atmosphere (shown in first column, from Table 2). All energies are in eV.

Table 9. Mean Source Altitude from Modified Atmospheres

Species	Species Modified						
	1 EUV	Low Ar	High Ar	Low CO_2	High CO_2	Low O	High O
O	159	159 (−0.1%)	159 (+0.1%)	157 (−1.5%)	161 (+1.0%)	159 (−0.1%)	160 (+0.2%)
CO_2	191	191 (−0.3%)	192 (+0.3%)	188 (−1.6%)	193 (+1.0%)	191 (+0.1%)	191 (−0.3%)
CO	178	178 (−0.1%)	178 (+0.1%)	176 (−1.2%)	180 (+1.1%)	178 (+0.1%)	179 (+0.3%)
C	181	181 (+0.1%)	181 (0%)	178 (−1.7%)	184 (+1.3%)	181 (0%)	182 (+0.2%)
N_2	205	208 (+1.8%)	203 (−0.8%)	199 (−2.7%)	205 (+0.2%)	201 (−2.0%)	206 (+0.8%)
N	192	192 (0%)	192 (0%)	189 (−1.7%)	194 (+1.2%)	193 (+0.2%)	192 (−0.1%)
Ar	192	193 (+0.3%)	191 (−0.6%)	189 (−1.5%)	195 (+1.3%)	192 (+0.1%)	192 (−0.1%)
Mean O	161	161 (−0.1%)	161 (+0.1%)	158 (−1.6%)	163 (+1.2%)	161 (−0.1%)	161 (+0.2%)
Mean C	181	181 (0%)	181 (+0.1%)	178 (−1.5%)	183 (+1.2%)	181 (0%)	181 (+0.2%)
Mean N	193	193 (0%)	192 (−0.1%)	189 (−1.7%)	195 (+1.1%)	193 (+0.1%)	192 (−0.1%)

Note. — The mean altitude that each species is lost from as the background atmosphere is modified. In all cases, the indicated species was changed by 25%. The percentage changes are relative to the 1 EUV atmosphere (shown in first column, from Table 3). All altitudes are in km.

Table 10. Model Yields for Modified Cross Sections

Species	Cross Section Modified				
	1 EUV	$+\sigma$ Ar	$-\sigma$ Ar	$+\sigma$ O	$-\sigma$ O
O	5.94	6.00 (+0.9%)	5.93 (−0.3%)	6.17 (3.8%)	5.54 (−6.8%)
CO_2	0.03	0.03 (+6.4%)	0.03 (−6.0%)	0.04 (37.1%)	0.03 (−14.4%)
CO	0.46	0.45 (−2.1%)	0.47 (+2.5%)	0.53 (15.5%)	0.38 (−18.1%)
C	1.46	1.46 (+0.1%)	1.48 (+1.1%)	1.57 (7.5%)	1.30 (−10.8%)
N_2	0.02	0.02 (+2.7%)	0.02 (−2.2%)	0.02 (30.1%)	0.01 (−25.1%)
N	1.10	1.09 (−0.7%)	1.11 (+0.7%)	1.23 (11.7%)	0.93 (−15.6%)
Ar	0.06	0.06 (+8.7%)	0.05 (−7.1%)	0.07 (13.4%)	0.05 (−17.0%)
Total O	6.47	6.51 (+0.7%)	6.46 (−0.1%)	6.78 (5.0%)	5.97 (−7.7%)
Total C	1.95	1.95 (−0.3%)	1.98 (+1.3%)	2.15 (9.9%)	1.71 (−12.5%)
Total N	1.14	1.13 (−0.6%)	1.14 (+0.6%)	1.28 (12.2%)	0.95 (−15.9%)
Total Yield	9.61	9.65 (+0.4%)	9.63 (+0.2%)	10.3 (6.9%)	8.68 (−9.7%)

Note. — The yield as the cross section of species are modified. In all cases, the indicated cross section is changed by 25%. The percentage changes are relative to the 1 EUV atmosphere (shown in first column, from Table 1).

Table 11. Model Energy Distribution

Energy	Modified Cross Section				
Sink	1 EUV	$+\sigma$ Ar	$-\sigma$ Ar	$+\sigma$ O	$-\sigma$ O
Electronic	402	398 (−1.0%)	404 (+0.6%)	376 (−6.5%)	437 (+8.8%)
Dissociation	252	252 (0%)	251 (−0.4%)	260 (+3.1%)	241 (−4.3%)
Thermal	146	148 (+1.5%)	143 (−1.9%)	158 (+7.9%)	132 (−9.8%)
Escaping	200	202 (+1.0%)	201 (+0.7%)	206 (+3.2%)	190 (−5.1%)

Note. — Ultimate location of the ion's initial keV of energy as various cross sections are modified. the indicated cross section is changed by 25%. The percentage changes are relative to the 1 EUV atmosphere (shown in first column, from Table 2). All energies are in eV.

Table 12. Mean Source Altitude for Modified Cross Sections

Species	Modified Cross Section				
	1 EUV	$+\sigma$ Ar	$-\sigma$ Ar	$+\sigma$ O	$-\sigma$ O
O	159	169 (−0.1%)	160 (+0.1%)	161 (1.2%)	157 (−1.8%)
CO_2	191	193 (+0.8%)	191 (−0.1%)	191 (0.2%)	192 (+0.2%)
CO	178	178 (+0.2%)	178 (−0.1%)	179 (0.5%)	178 (−0.3%)
C	181	181 (−0.1%)	181 (−0.2%)	182 (0.3%)	180 (−0.4%)
N_2	205	205 (0%)	206 (+0.4%)	206 (0.8%)	202 (−1.5%)
N	192	192 (−0.1%)	192 (−0.3%)	193 (0.3%)	191 (−0.4%)
Ar	192	194 (+1.1%)	190 (−1.0%)	193 (0.5%)	192 (−0.2%)
Mean O	161	161 (0%)	161 (+0.1%)	163 (1.3%)	158 (−1.8%)
Mean C	181	181 (0%)	180 (−0.2%)	181 (0.3%)	180 (−0.4%)
Mean N	193	192 (−0.1%)	192 (−0.3%)	193 (0.3%)	192 (−0.5%)

Note. — The mean altitude that each species is lost from as model cross sections are modified. the indicated cross section is changed by 25%. The percentage changes are relative to the 1 EUV atmosphere (shown in first column, from Table 3). All altitudes are in km.

Table 13. Model Yields for Varied Scattering Functions

Species	Scattering Function Modified						
	1 EUV	Forward Ar	Backward Ar	Forward CO_2	Backward CO_2	Forward O	Backward O
O	5.94	5.95 (+0.1%)	5.90 (−0.7%)	5.94 (0%)	5.87 (−1.2%)	5.94 (−0.1%)	5.92 (−0.5%)
CO_2	0.03	0.03 (+0.7%)	0.03 (+1.3%)	0.03 (+11.0%)	0.03 (−2.0%)	0.03 (−2.3%)	0.03 (−11.7%)
CO	0.46	0.47 (+1.2%)	0.46 (−0.6%)	0.48 (+5.0%)	0.43 (−7.8%)	0.46 (−1.3%)	0.46 (−0.3%)
C	1.46	1.45 (−0.5%)	1.46 (+0.2%)	1.46 (0%)	1.46 (+0.1%)	1.46 (−0.3%)	1.45 (−0.5%)
N_2	0.02	0.02 (−6.0%)	0.02 (−2.7%)	0.02 (−7.1%)	0.02 (−6.0%)	0.02 (−2.2%)	0.02 (+12.6%)
N	1.10	1.09 (−1.3%)	1.10 (+0.1%)	1.11 (+0.8%)	1.08 (−2.1%)	1.10 (−0.5%)	1.11 (+0.6%)
Ar	0.06	0.06 (−0.5%)	0.06 (+5.9%)	0.06 (+9.4%)	0.06 (+6.3%)	0.06 (+0.5%)	0.06 (+11.1%)
Total O	6.47	6.48 (+0.2%)	6.42 (−0.7%)	6.50 (+0.5%)	6.35 (−1.7%)	6.45 (−0.2%)	6.43 (−0.6%)
Total C	1.95	1.95 (−0.1%)	1.95 (0%)	1.98 (+1.3%)	1.92 (−1.8%)	1.94 (−0.5%)	1.94 (−0.7%)
Total N	1.14	1.12 (−1.5%)	1.14 (0%)	1.14 (+0.5%)	1.11 (−2.3%)	1.13 (−0.6%)	1.15 (+1.0%)
Total Yield	9.61	9.61 (−0.1%)	9.57 (−0.4%)	9.68 (+0.7%)	9.44 (−1.7%)	9.56 (−0.3%)	9.58 (−0.3%)

Note. — The yield as the scattering function for various species is modified. A "Forward" is one where the scattering function is more forward than normal, while a "Backwards" one is one that scatters more rearward (see the text for more details). All values are compared to the 1 EUV case (shown in the first column, from Table 1).

Table 14. Model Energy Distribution for Modified Scattering Functions

Energy Sink	Scattering Function Modified						
	1 EUV	Forward Ar	Backward Ar	Forward CO_2	Backward CO_2	Forward O	Backward O
Electronic	402	405 (+0.8%)	400 (−0.5%)	401 (−0.2%)	402 (0%)	403 (+0.3%)	404 (+0.5%)
Dissociation	252	253 (+0.2%)	252 (−0.1%)	250 (−0.9%)	256 (+1.4%)	252 (+0.2%)	252 (−0.2%)
Thermal	146	142 (−2.5%)	148 (+1.3%)	145 (−0.7%)	146 (+0.2%)	146 (0%)	146 (−0.1%)
Escaping	200	200 (0%)	200 (+0.1%)	204 (+2.0%)	196 (−1.9%)	199 (−0.7%)	199 (−0.8%)

Note. — Ultimate location of the ion's initial keV of energy as the indicated scattering functions are modified. A "Forward" case is one where the particle is more likely to scatter forward, a "Backwards" one is the opposite (see the text for more details). All values are compared to the 1 EUV case (shown in the first column, from Table 2). All energies are in eV.

Table 15. Mean Source Altitude as Cross Sections are Modified

Species	Scattering Function Modified						
	1 EUV	Forward Ar	Backward Ar	Forward CO_2	Backward CO_2	Forward O	Backward O
O	159	159 (−0.1%)	159 (0%)	160 (+0.1%)	159 (−0.2%)	159 (−0.1%)	159 (−0.1%)
CO_2	191	192 (+0.3%)	191 (+0.2%)	192 (+0.3%)	191 (+0.1%)	190 (−0.6%)	191 (0%)
CO	178	178 (0%)	179 (+0.5%)	177 (−0.4%)	178 (0%)	178 (0%)	178 (+0.1%)
C	181	181 (0%)	181 (+0.1%)	181 (0%)	181 (−0.1%)	181 (+0.1%)	181 (0%)
N_2	205	205 (+0.1%)	205 (+0.1%)	205 (+0.2%)	208 (+1.8%)	205 (0%)	206 (+0.7%)
N	192	192 (+0.1%)	192 (+0.1%)	192 (−0.1%)	192 (+0.1%)	192 (+0.1%)	192 (+0.1%)
Ar	192	189 (−1.7%)	196 (+1.8%)	192 (−0.2%)	193 (+0.6%)	192 (−0.1%)	193 (+0.3%)
Mean O	161	161 (−0.1%)	161 (+0.1%)	161 (+0.1%)	161 (−0.2%)	161 (−0.1%)	161 (−0.1%)
Mean C	181	181 (0%)	181 (+0.1%)	180 (−0.1%)	181 (−0.1%)	181 (0%)	181 (0%)
Mean N	193	193 (+0.1%)	193 (+0.1%)	192 (+0.2%)	193 (+0.1%)	193 (0%)	193 (+0.1%)

Note. — The mean altitude that each species is lost from as the cross section for individual collisions is modified. A "Forward" one is one that has more forward scattering angles (see the text for more details). All values are compared to the 1 EUV case (shown in the first column, from Table 3). All altitudes are in km.

Table 16. Integrated Losses

	6 EUV	3 EUV	1 EUV	Total Loss
Sputtered O	1.0×10^{28}	6.6×10^{26}	2.3×10^{24}	1.4 bar
Exospheric O	1×10^{27}	5×10^{26}	8×10^{25}	0.3 bar
Pickup O^+	3×10^{27}	4×10^{26}	6×10^{24}	0.5 bar
Sputtered CO_2	2.2×10^{27}	1.6×10^{26}	6.9×10^{23}	0.8 bar
Escaped H_2O	1.0×10^{28}	1.2×10^{27}	8.7×10^{25}	50 m

Note. — The integrated loss flux, in particles per second, for each epoch. The "Sputtered O" line contains all O atoms, regardless of the actual species. "Exospheric O" and "Pickup O^+" refer to two non-sputtering loss processes (Luhmann *et al.* 1992). "Sputtered CO_2" assumes that each carbon atom lost represents the loss of a CO_2 molecule (and is balanced by two O atoms). "Escaped H_2O" assuming that any O not needed to balance a C atom represents the loss of a water molecule. The last column is the integrated loss over the period modeled.

Table 17. Selected Scattering Functions

			Henyey–Greenstein parameters		
		Single	Double		
		g	a	g_1	g_2
O + O	60 eV		0.04	0.25	0.99
	200 eV		0.015	0.25	0.99
	600 eV		0.003	0.25	0.99
O + H			0.4	0.18	0.95
$O + CO_2$	$\rightarrow O + CO_2$				
	60 eV	0.72			
	200 eV	0.85			
	600 eV	0.85			
	$\rightarrow O + O + CO$				
	O^* 60 eV	−0.23			
	200 eV	0.25			
	600 eV	0.54			
	O^a 60 eV	0.2			
	200 eV		0.52	−0.43	−0.02
	600 eV		0.16	−0.93	−0.5
	CO 60 eV	−0.37			
	200 eV	−0.74			
	600 eV	−0.9			

Fig. 1.— Sputtering Process. In step 1, ions are accelerated by the interactions of the ionosphere, solar EUV and solar wind. In step 2, the ions impact the upper atmosphere and collisionally transfer energy and momentum, ejecting part of the atmosphere.

Fig. 2.— Present (1 EUV) Atmosphere Model. Number densities for the various species in the present atmosphere (Nair *et al.* 1994). This has been extended isostatically (see also figure 3).

Fig. 3.— Present (1 EUV) Atmosphere Structure. Temperature (solid line) and pressure (dashed line) in the present atmosphere (Nair *et al.* 1994). The step in temperature at 240 km is where the isostatic extension was added.

Fig. 4.— Past (3 EUV and 6 EUV) Atmosphere Models. Number densities used for the 3 EUV and 6 EUV atmospheres (Zhang *et al.* 1993). This has been extended isostatically.

Fig. 5.— Source Altitudes for Escaping Particles at 6 EUV. The altitude that each escaping particle is accelerated from (it may have further collisions before actually escaping). Each curve is plotted as a fraction of all the molecules of that species to escape the atmosphere. The horizontal dashed line is the CO_2 homopause for the atmosphere.

Fig. 6.— Source Altitudes for Escaping Particles at 3 EUV. The altitude that each escaping particle is accelerated from (it may have further collisions before actually escaping). Each curve is plotted as a fraction of all the molecules of that species to escape the atmosphere. The horizontal dashed line is the CO_2 homopause for the atmosphere.

Fig. 7.— Source Altitudes for Escaping Particles at 1 EUV. The altitude that each escaping particle is accelerated from (it may have further collisions before actually escaping). Each curve is plotted as a fraction of all the molecules of that species to escape the atmosphere. The horizontal dashed line is the CO_2 homopause for the atmosphere.

Table 17—Continued

		Henyey–Greenstein parameters			
		Single	Double		
		g	a	g_1	g_2
$\rightarrow$ O + 2 O + C					
O*	60 eV	−0.48			
	200 eV	0.07			
	600 eV	0.49			
O	60 eV	0.2			
	200 eV		0.52	−0.43	−0.02
	600 eV		0.16	−0.93	−0.5
C	60 eV	0.51			
	200 eV	−0.02			
	600 eV	−0.35			

*Function for impacting fast molecule

[a]Due to this resulting in 3 particles, the scattering angle is not determined for this O atom.

Note. — The Henyey–Greenstein parameters (either for a single HG function or for a double HG function) used for the indicated collisions. (Johnson and Liu 1998; Johnson *et al.* 1999; Gurwell and Yung 1993)

Fig. 8.— Integrated Loss over Time. Loss fluxes (particles per second) integrated over Mars. "a" is the total H_2O loss rate. "b" is the Exospheric loss rate. "c" is the O sputtering flux from the model. "d" is the O sputtering flux from Luhmann *et al.* (1992). "e" is the CO_2 sputtering flux from the model. "f" is the CO_2 sputtering flux from Luhmann *et al.* (1992).

Fig. 9.— O + O, O + N_2 and O + CO Cross Sections. (Ishimoto *et al.* 1986; Johnson and Liu 1998).

Fig. 10.— O + CO_2 Cross Sections. (Johnson and Liu 1998).

Fig. 11.— CO + CO_2 Cross Sections. (Johnson and Liu 1998).

Sputtering Process

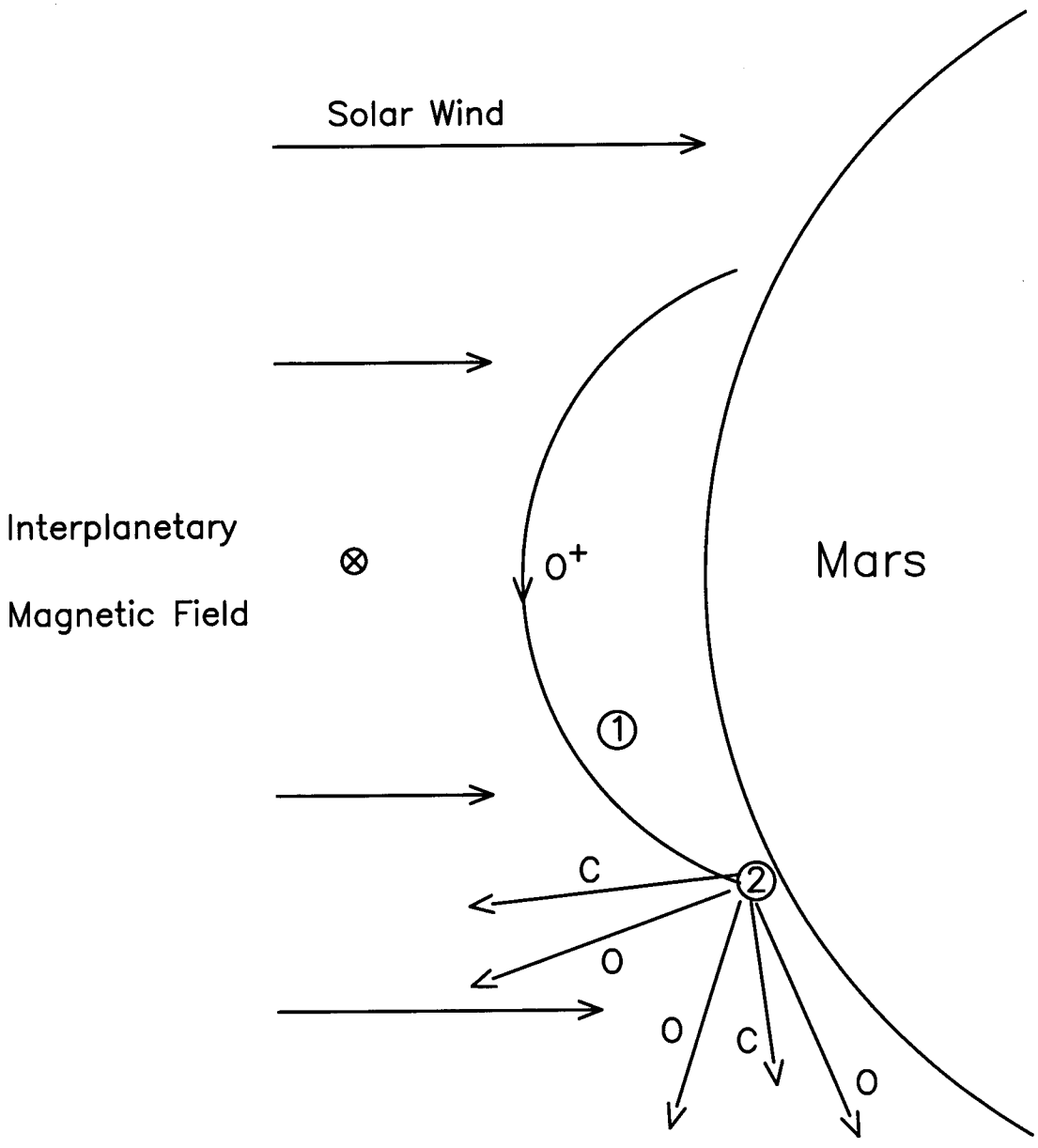

Fig 1

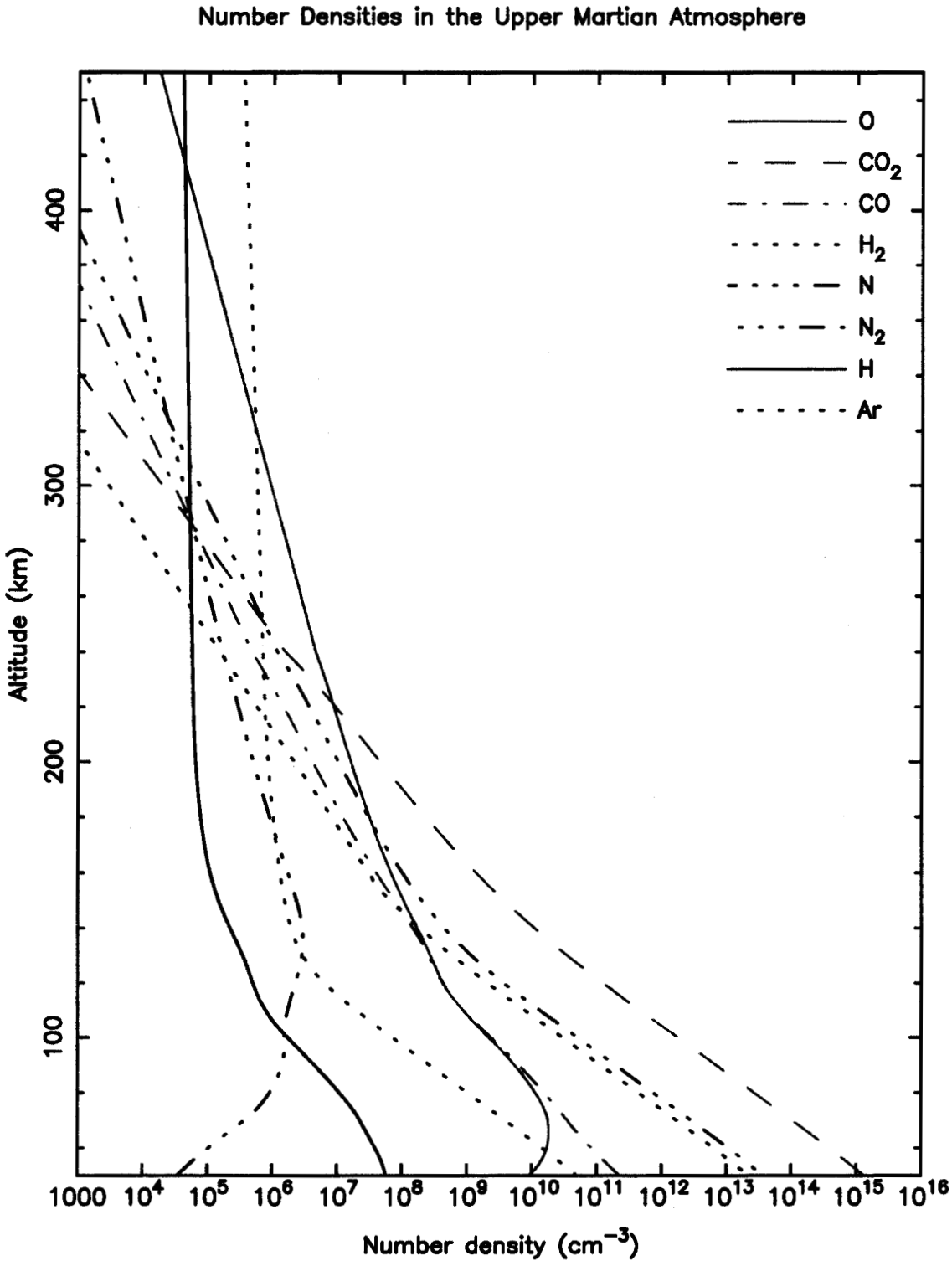
Number Densities in the Upper Martian Atmosphere
O
CO_2
CO
H_2
N
N_2
H
Ar
Altitude (km)
100
200
300
400
1000
10^4
10^5
10^6
10^7
10^8
10^9
10^{10}
10^{11}
10^{12}
10^{13}
10^{14}
10^{15}
10^{16}
Number density (cm^{-3})

Fig 2

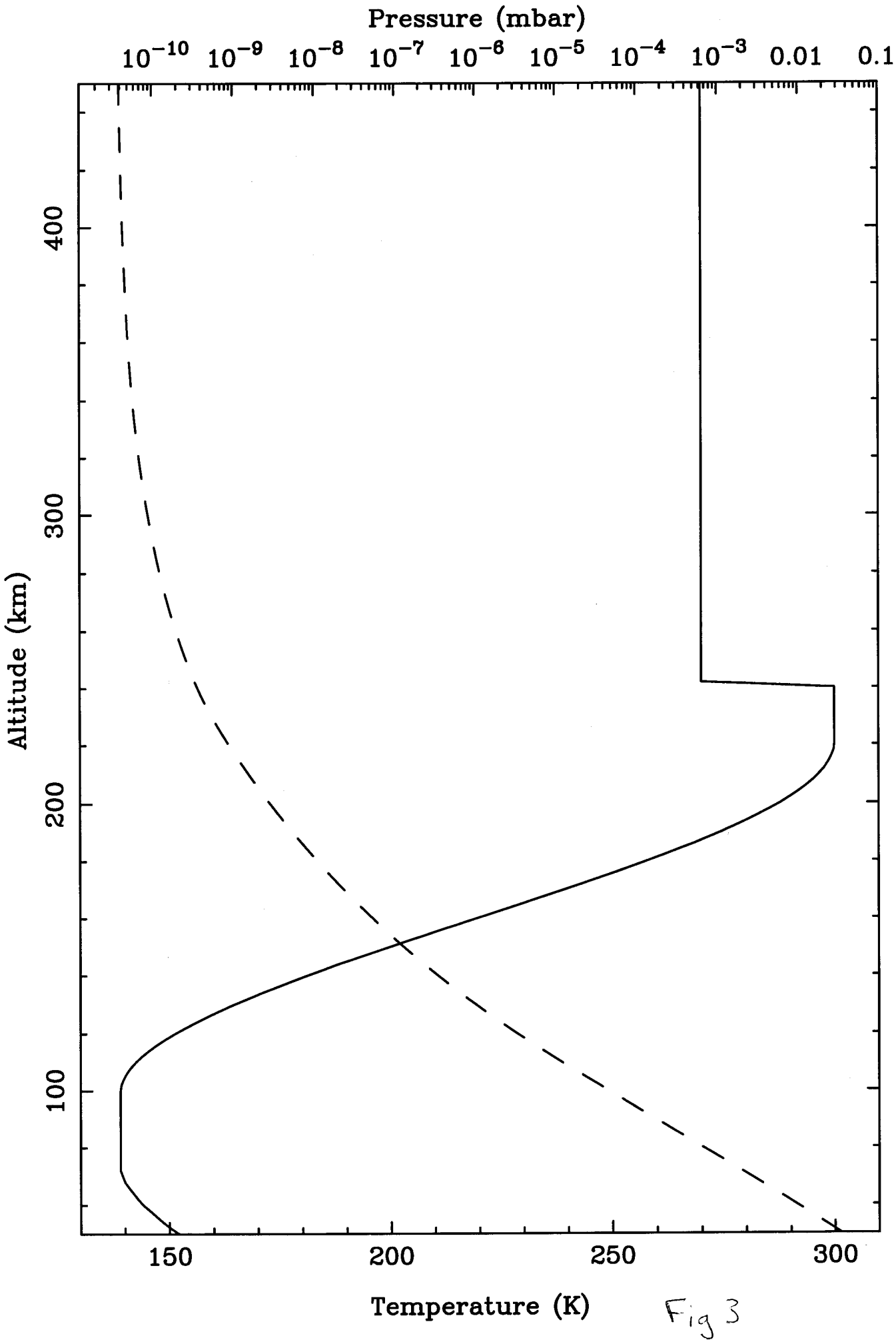
Pressure (mbar)
10^{-10} 10^{-9} 10^{-8} 10^{-7} 10^{-6} 10^{-5} 10^{-4} 10^{-3} 0.01 0.1
Altitude (km)
100
200
300
400
150
200
250
300
Temperature (K)

Fig 3

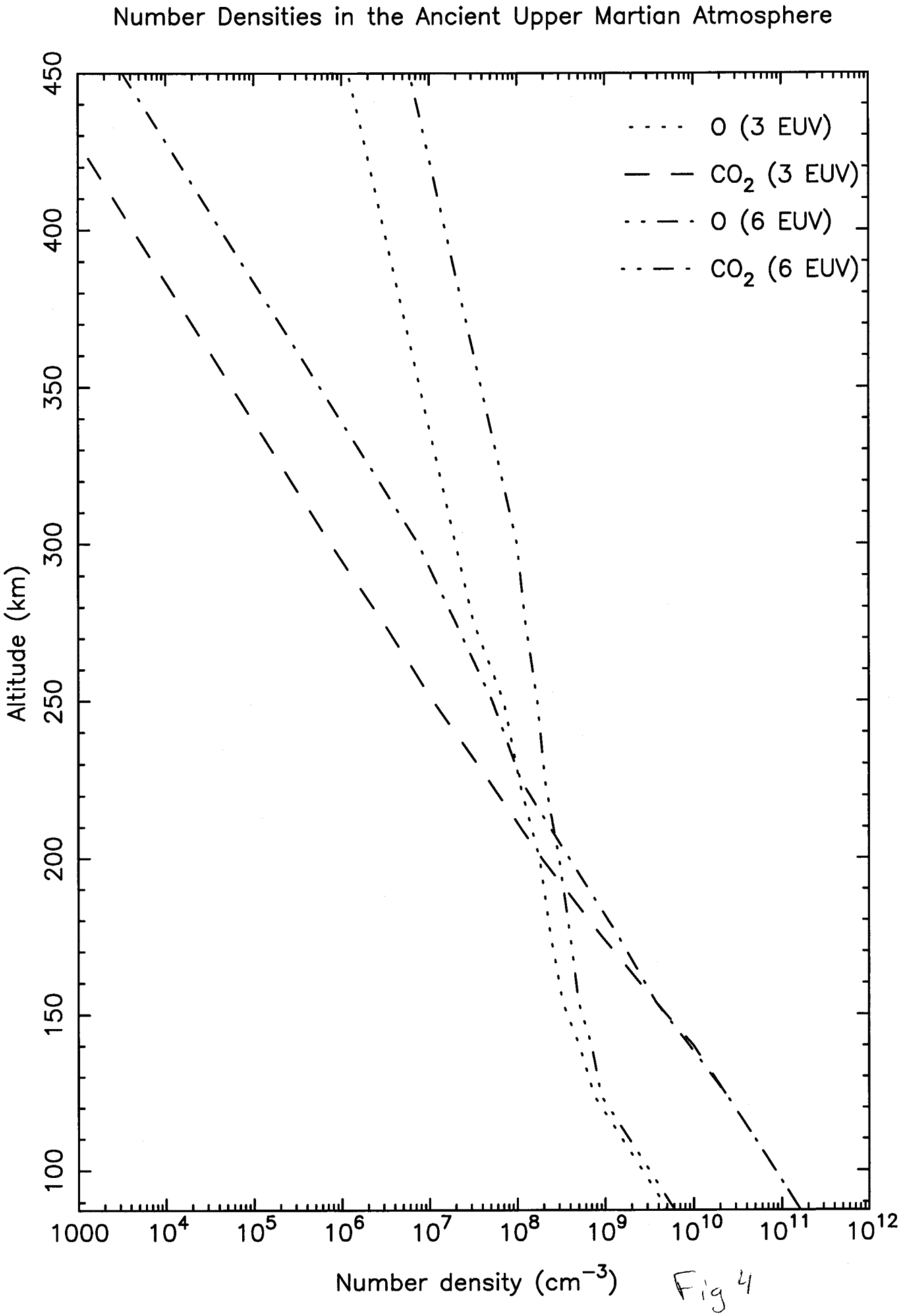
Number Densities in the Ancient Upper Martian Atmosphere
O (3 EUV)
CO_2 (3 EUV)
O (6 EUV)
CO_2 (6 EUV)
Altitude (km)
100
150
200
250
300
350
400
450
1000
10^4
10^5
10^6
10^7
10^8
10^9
10^{10}
10^{11}
10^{12}
Number density (cm^{-3})

Fig 4

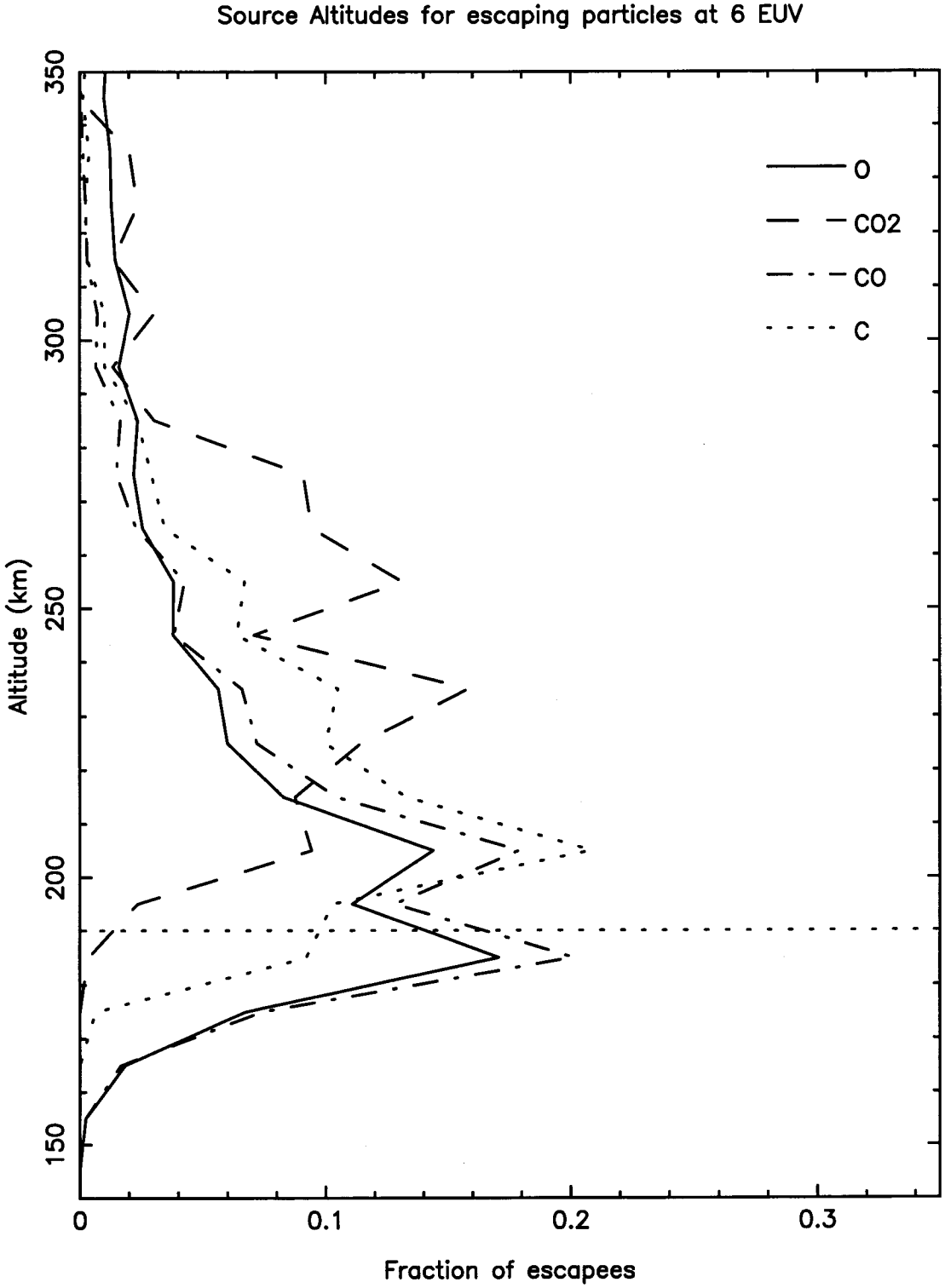
Source Altitudes for escaping particles at 6 EUV
Altitude (km)
350
300
250
200
150
0
0.1
0.2
0.3
Fraction of escapees
O
CO2
CO
C

Fig 5

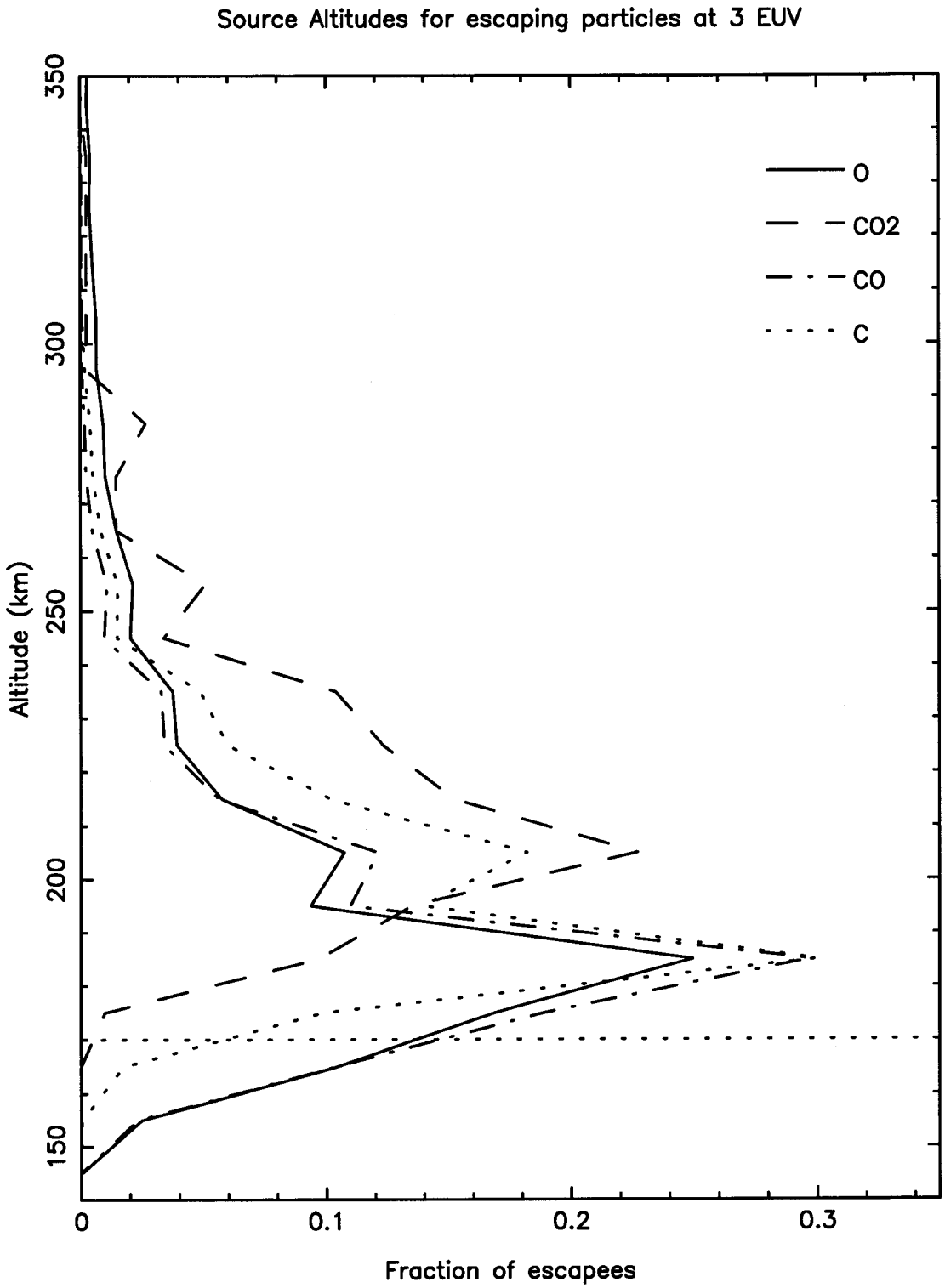
Source Altitudes for escaping particles at 3 EUV
Altitude (km)
350
300
250
200
150
0
0.1
0.2
0.3
Fraction of escapees
O
CO2
CO
C

Fig 6

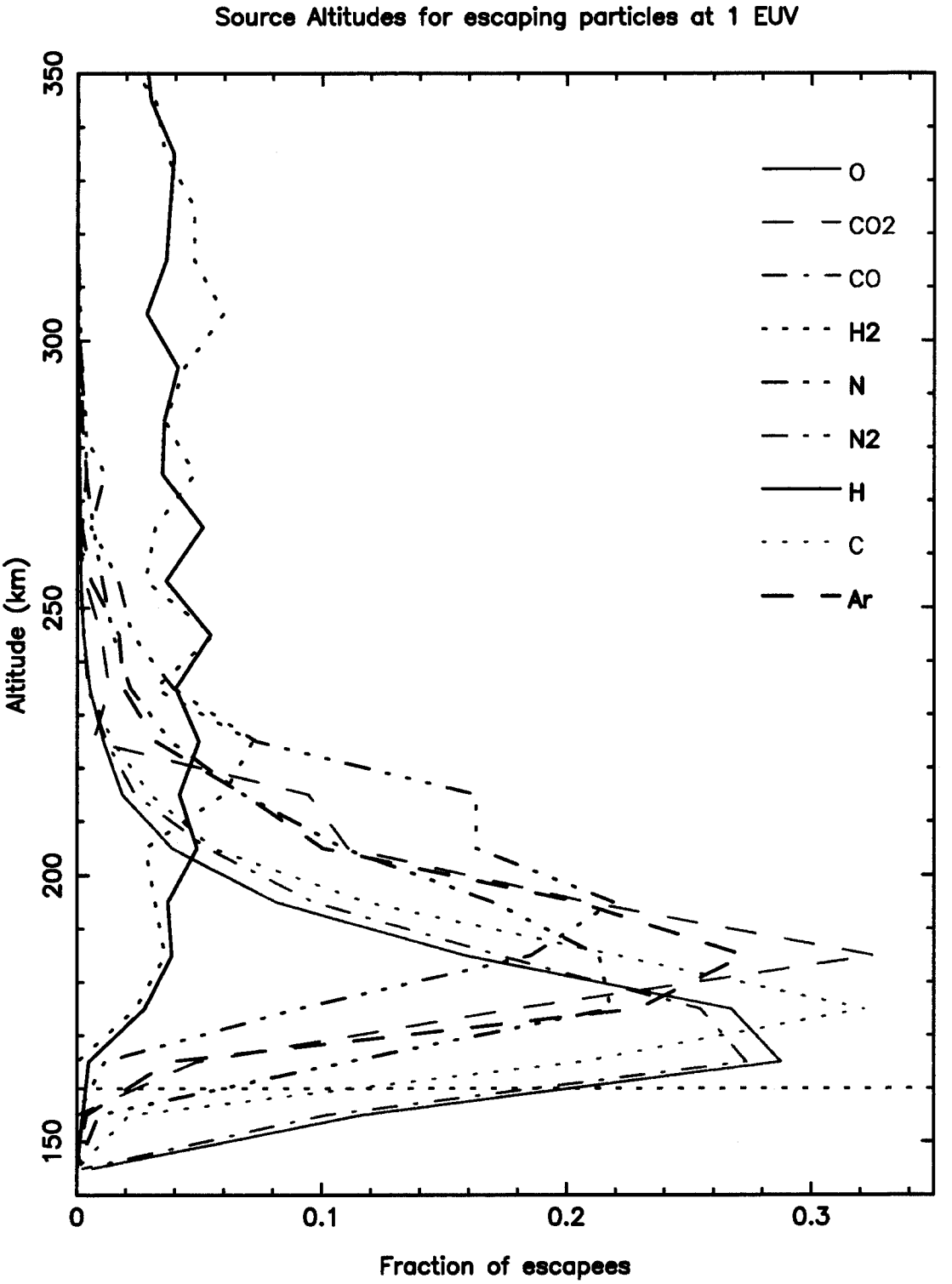
Source Altitudes for escaping particles at 1 EUV
Altitude (km)
350
300
250
200
150
0
0.1
0.2
0.3
Fraction of escapees
O
CO2
CO
H2
N
N2
H
C
Ar

Fig 7

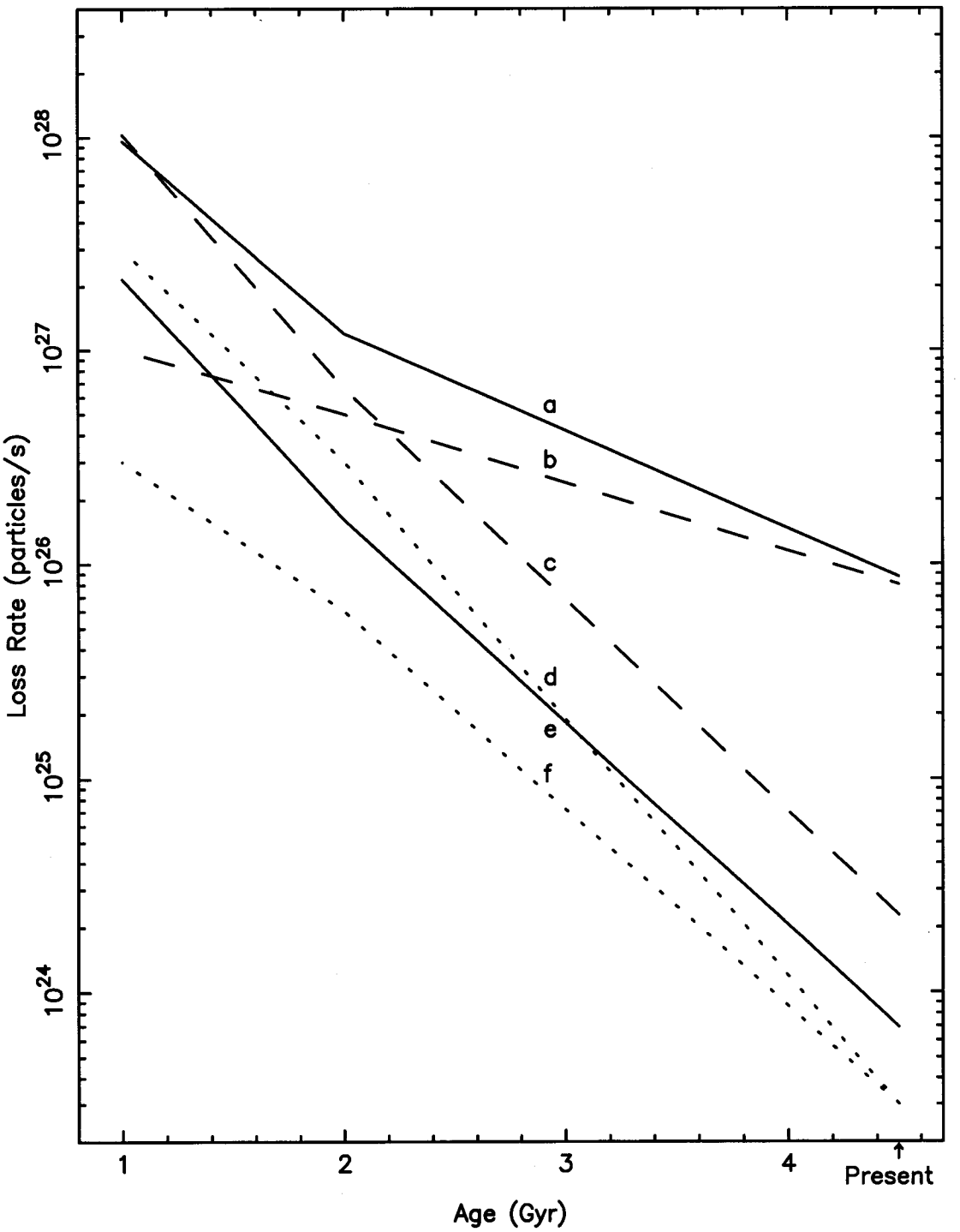
Loss Rate (particles/s)
10^{28}
10^{27}
10^{26}
10^{25}
10^{24}
a
b
c
d
e
f
1
2
3
4
Present
Age (Gyr)

Fig 8

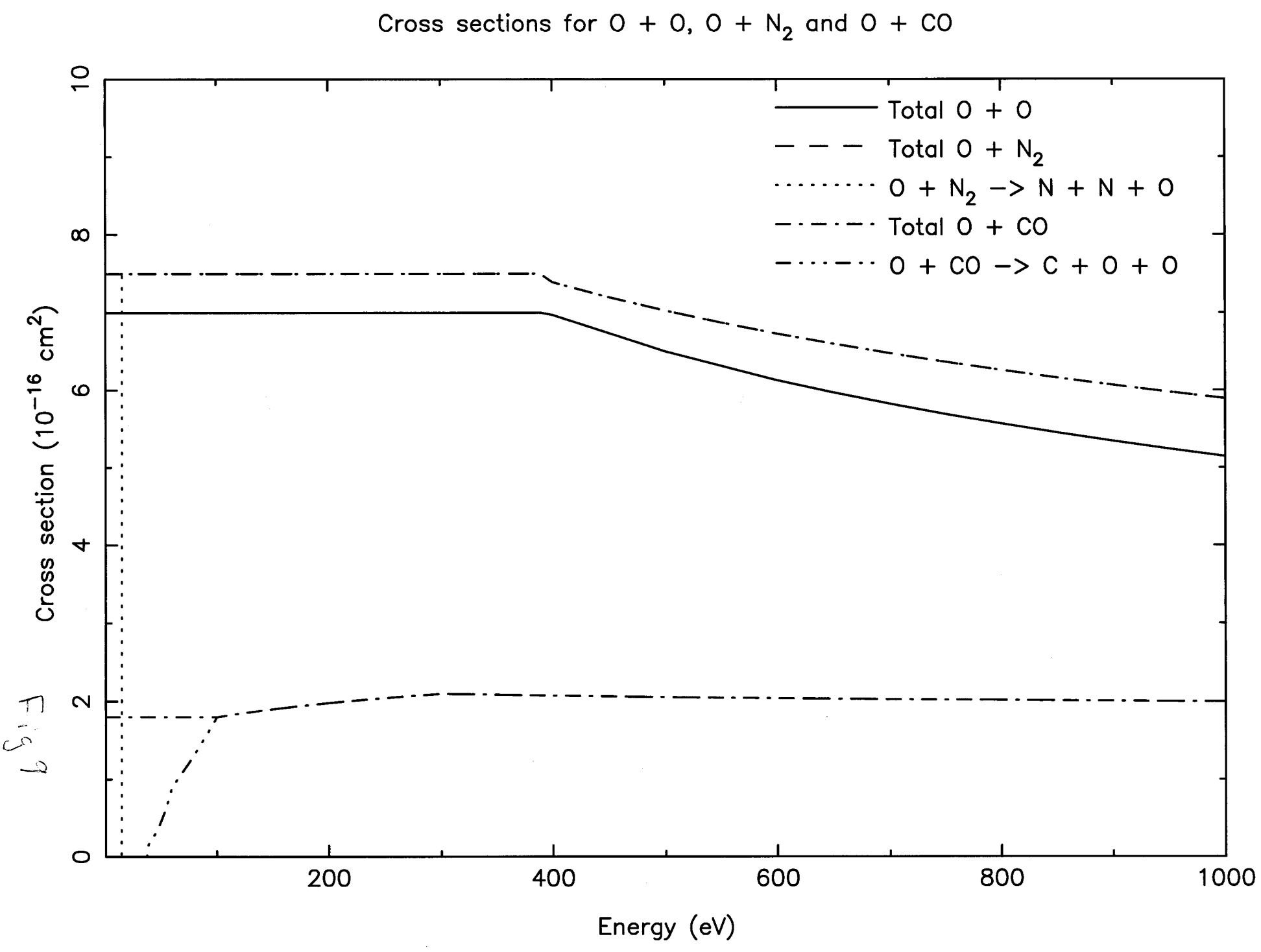
Cross sections for O + O, O + N_2 and O + CO
Total O + O
Total O + N_2
O + N_2 -> N + N + O
Total O + CO
O + CO -> C + O + O
Cross section (10^{-16} cm^2)
Energy (eV)
0
2
4
6
8
10
200
400
600
800
1000

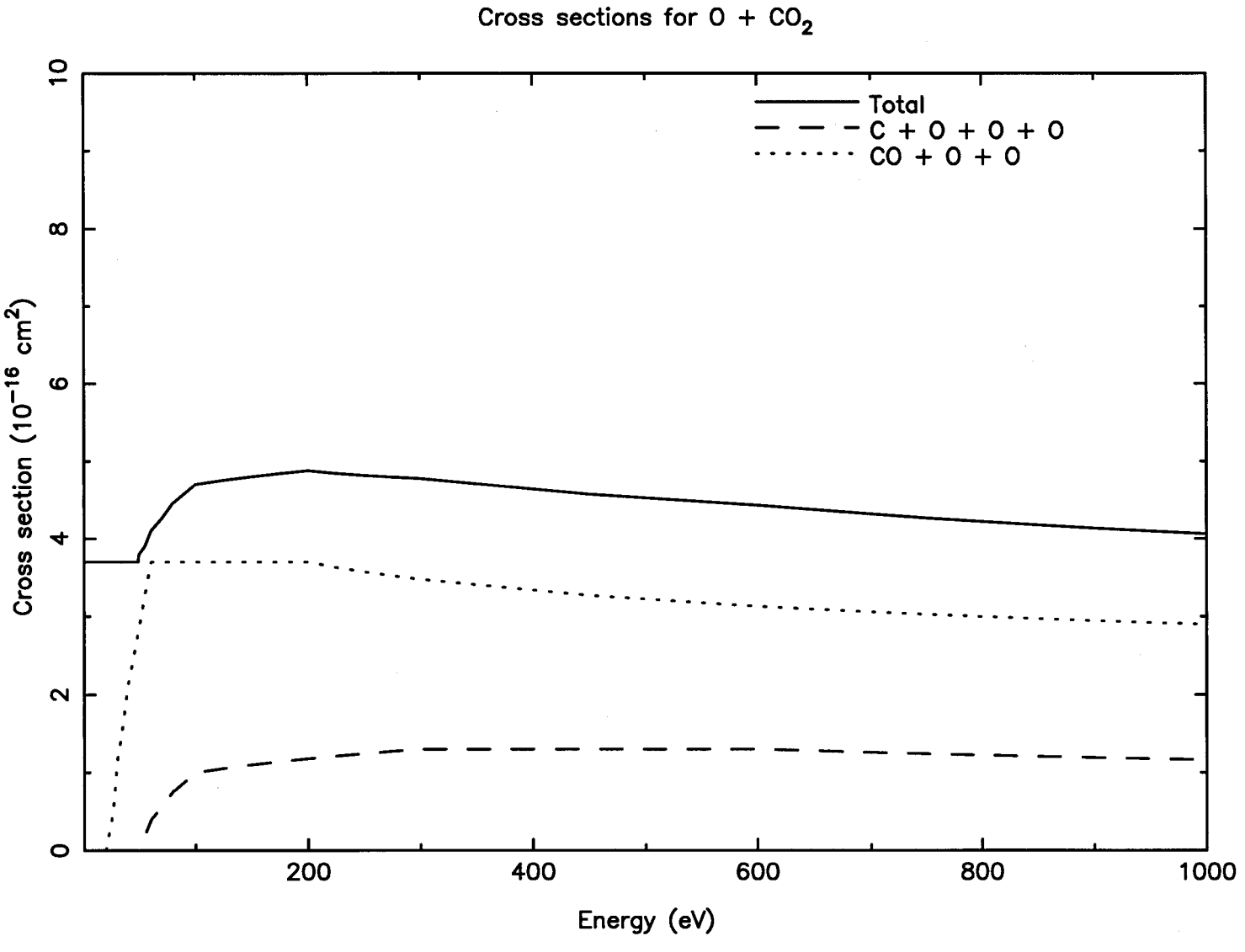
Cross sections for O + CO_2
Total
C + O + O + O
CO + O + O
Cross section (10^{-16} cm^2)
0
2
4
6
8
10
200
400
600
800
1000
Energy (eV)

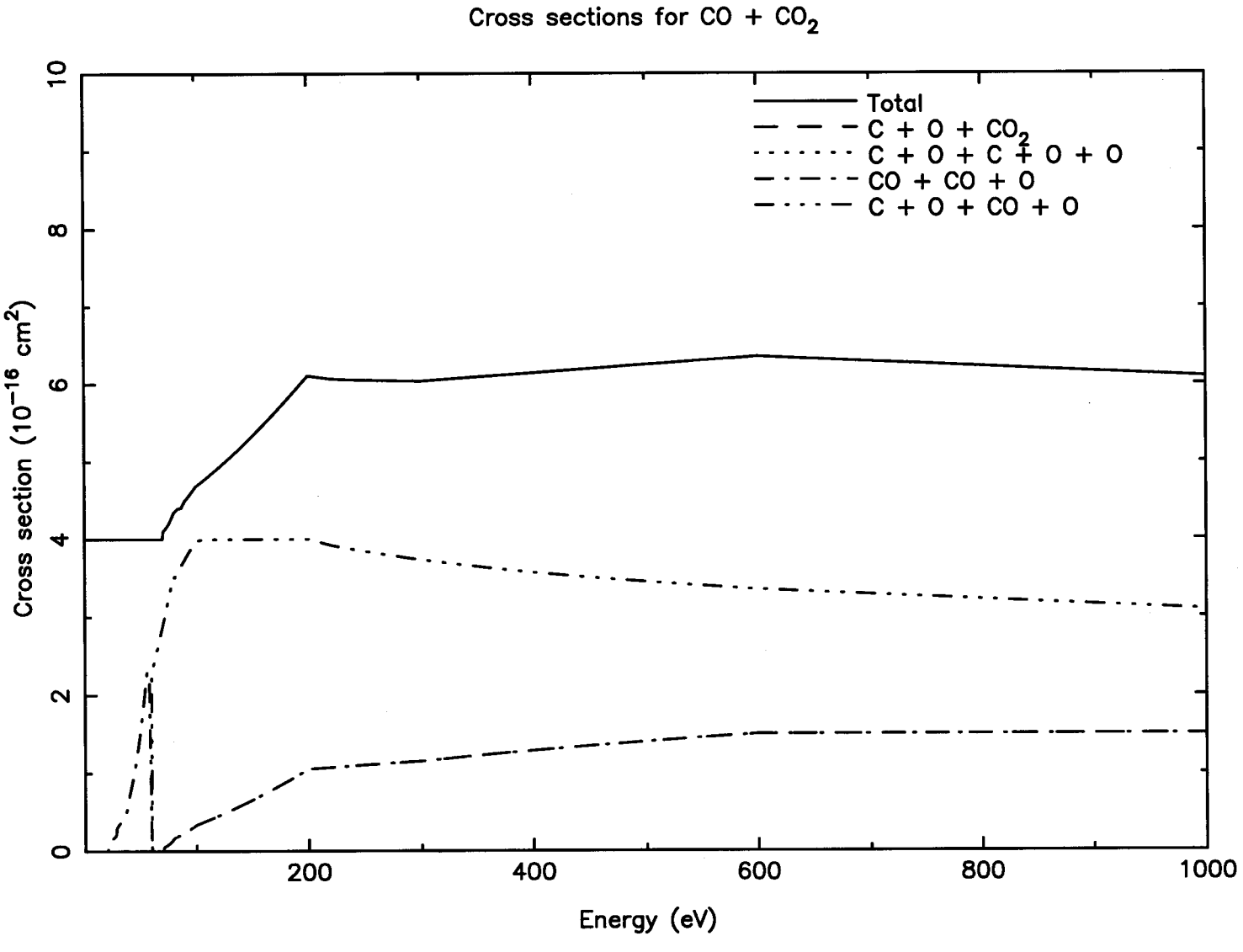
Cross sections for CO + CO2
Total
C + O + CO2
C + O + C + O + O
CO + CO + O
C + O + CO + O
Cross section (10^-16 cm^2)
Energy (eV)
0
2
4
6
8
10
200
400
600
800
1000